INFLUENCE OF HIGH ENERGY RADIATION ON THE OPTICAL AND LUMINESCENT PROPERTIES OF PHTHALOCYANINE THIN FILMS

A Minor Research Project Report
Submitted to the

UNIVERSITY GRANTS COMMISSION

BY
Dr. VINU T. VADAKEL

ASSISTANT PROFESSOR

DEPARTMENT OF PHYSICS

ST ALOYSIUS' COLLEGE

EDATHUA, KERALA

1883-MRP/14-15/KLMG019/UGC-SWRO

Acknowledgment

I would like to thank God Almighty for his abundant blessings throughout my project work.

It is with pleasure that we express our sincere gratitude to Dr. C.S Menon for his valuable guidance and keen interest throughout the progress of the work which helped in clarifying the ideas.

I acknowledge with thanks the support in the form of financial assistance from university grants commission, ***New Delhi*** *for sanctioning the project.*

I express my sincere gratitude to all faculties of Dept.of physics, St.Aloysius College Edathua for their constant encouragement.

We are thankful to Mahatma Gandhi University for providing some of the experimental facilities.

Dr. VINU T. VADAKEL

ABSTRACT

The present investigation comprises of the studies on the optical characterisation of H_2PcOC_8, $ZnPcOC_8$ and $CuPcOC_8$ thin films. The effects of gamma irradiation on the optical and electrical properties are also studied. Powdered samples of spectroscopically pure H_2PcOC_8, $ZnPcOC_8$ and $CuPcOC_8$ obtained from Sigma Aldrich Chemical Company, USA are used as the source material. Thin films are prepared at a base pressure of 10^{-6} m. bar using Hind Hivac 12 A4 thermal evaporation plant. Thicknesses of the films are measured using Tolansky's multiple beam interference technique. The effects of gamma irradiations on the optical and electrical properties are also studied by irradiating the thin films with gamma rays using Gamma ray Chamber 5000.

CONTENTS

CHAPTER 1

REVIEW ON THE PROPERTIES OF SUBSTITUTED PHTHALOCYANINE THIN FILMS

1.1 Introduction to thin film technology

In recent years, thin film science has grown into a major research area. The importance of coatings and the synthesis of new materials for industry have resulted in a tremendous increase of innovative thin film processing technology. Currently, this development goes hand- in- hand with the explosion of scientific and technological break- through in microelectronics, optics and nanotechnology [1]. Another major field comprises process technologies for films with thickness ranging from one to several microns. These films are essential for multitudes of production such as thermal barrier coatings and wear protections, enhancing service life of tools and materials against environmental influences [2- 3]. Presently, rapidly changing needs for thin film materials and devices are creating new opportunities for the development of new processes, materials and technologies. Results of combined experimental and theoretical investigations are a prerequisite for the development of new thin film systems and the tailoring of their microstructure and performance. The major exploitation of thin film science is still in the field of microelectronics. However, there are growing applications in other areas like thin films for optical and magnetic devices, electrochemistry, protective and decorative coatings and catalysis.

1.2 Organic semiconductors

Organic semiconductors have shown immense potential in terms of their numerous technological applications which were earlier dominated by inorganic semiconductors. These applications started off with electroluminescent devices, but have since diversified to include microelectronic devices and integrated circuits. The electronic conductivity of these materials lies between that of metals and insulators, spanning a broad range of 10^{-9} to 10^{3} $(\Omega\ cm)^{-1}$.

Known organic semiconductors can be broadly classified into two groups on the basis of their molecular weight:

1. Conjugated polycyclic compounds of molecular weight less than 1000.
2. Heterocyclic polymers with molecular weight greater than 1000.

Polymers are easily deposited as thin films on large areas making them valuable semiconducting materials. Nevertheless, they suffer from a major drawback in that they are not highly soluble in organic solvents, and they lose their mobility upon functionalization to enhance solubility. This has been a major driving force behind the research on small molecular semiconductors. With molecular semiconductors, it is possible to control charge transport in a simpler way by modification of various molecular parameters. For example, the ability of these molecules to pack into well-organized polycrystalline films leads to higher mobility compared to polymeric semiconductors.

1.3 Phthalocyanines

Phthalocyanine (Pc) is a symmetrical 18π- electron aromatic macrocycle, in which more than 70 different metal and also non- metal ions can be incorporated, closely related to the naturally occuring porphyrins.

Like the porphyrins, the Pc macrocycle can play host to over seventy different metal ions in its central cavity. The basic 18π- electron structure in metal free and metallo Phthalocyanine (MPc) molecules has very rich molecular orbitals and available energy levels. The populated ground highest occupied molecular orbital (HOMO) and singlet highest occupied molecular orbital (SHOMO) levels are a_{14} (π) and a_{24} (π) and the first excited lowest unoccupied molecular orbitals (LUMO) level is e_g (π*). In Phthalocyanines the transitions between these molecular orbitals are the reason for producing different absorption maxima in the absorption spectra. Since its discovery, Pc and its derivatives have been extensively used as colorants. More recently they have been employed in several 'hi-tech' applications such as photo conducting material in laser printers and the light absorbing layer in CDs. They are also used as photosensitisers in laser cancer therapy, as nonlinear optical materials and as industrial catalysts. The synthesis and applications of Pc materials is a very dynamic and multidisciplinary field of research.

1.4 Properties of substituted phthalocyanines

Unsubstituted phthalocyanine is the parent compound of a series of derivatives, (Figure 1.1), that possess many remarkable properties [4- 6]. An intense π-π^* absorption in the visible region of the spectrum, the Q- band, renders them attractive as blue green colorants. Indeed, the brightness of the colours, coupled with exceptional chemical and thermal stability, has led to extensive manufacture of particular examples as commercial dyes and pigments. Others have found use as oxidation catalysts for several manufacturing processes [7]. However, the cyclic 18π- electron system of these compounds also provides the basis of a variety of interesting photophysical and conducting properties [4- 6]. These ensure that Pcs are important functional molecular materials much valued for applications in

contemporary and emerging technologies. They are used as charge carriers in photocopiers, as dyes in laser printers [8- 9] and as laser absorbers within optical data storage systems [10- 11]. They are also promising materials for applications in solar cells [12- 13], gas sensors [14- 15] and nonlinear optical and optical limiting devices [16- 18]. Furthermore, particular examples are recognised as being important singlet oxygen photosensitizers for the photodynamic therapy of cancer [19- 20], others as a possible therapy for transmissible spongiform encephalopathies [21].

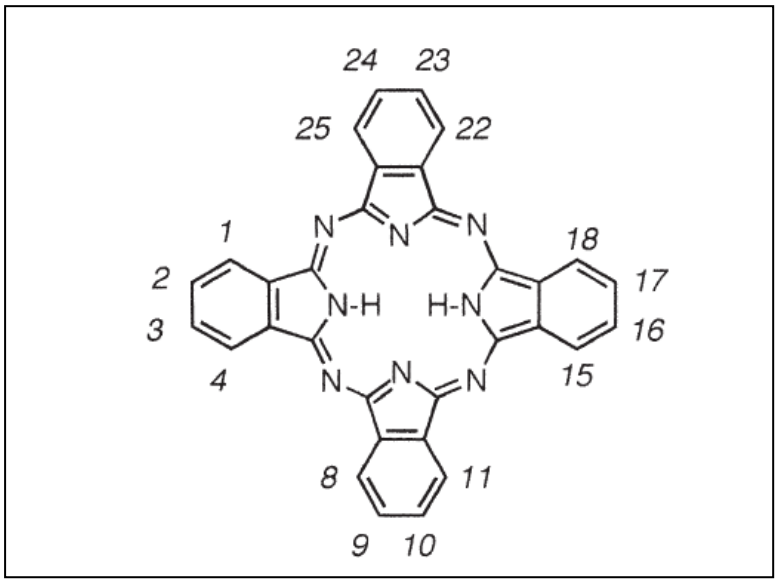

Fig. 1.1 Phthalocyanine (or metal- free phthalocyanine) showing the ring numbering. Replacement of the central N- H protons by a metal ion leads to metallated derivatives

Many of these developments have been possible because of the ease of tuning the properties of the ring system. Two principle strategies are available. One is to replace the N- H protons in the centre of the ring by a metal ion or metalloid element. The other is to introduce substituent groups onto the benzenoid rings. The latter is particularly important for conferring solubility in a variety of solvents and also for red- shifting the Q- band.

Substituents can be introduced via electrophilic substitution of the Pc ring, but a lack of scope and regioselectivity frequently makes it more attractive to introduce substituents onto the precursor to the ring. For research purposes, particular use is made of derivatised phthalonitriles. These undergo base catylysed cyclotetramerisation followed by two electron reduction step to form the Pc nucleus. Figure 1.3 shows three series of substituted Pc derived from their appropriate phthalonitrile precursors. A monosubstituted phthalonitrile provides a tetra- substituted macrocycle, which is typically formed as an isomer mixture. Single component products, however, bearing eight substituents are formed from the corresponding di- substituted phthalonitriles. Figure 1.2 shows two such series of Pc referred to as the peripheral (2, 3, 9, 10, 16, 17, 23, 24) and nonperipheral (1, 4, 8, 11, 15, 18, 22, 25) octa- substituted derivatives. Thus in the present study, the materials selected are 2, 3, 9, 10, 16, 17, 23, 24 Octakis (octyloxy) Phthalocyanine (H_2PcOC_8), 2, 3, 9, 10, 16, 17, 23, 24 Octakis (octyloxy) Zinc Phthalocyanine ($ZnPcOC_8$), 2, 3, 9, 10, 16, 17, 23, 24 Octakis (octyloxy) Copper Phthalocyanine ($CuPcOC_8$). The molecular formula of octyloxy group is $C_8H_{17}O$, which is substituted in the peripheral 2, 3, 9, 10, 16, 17, 23, 24 positions.

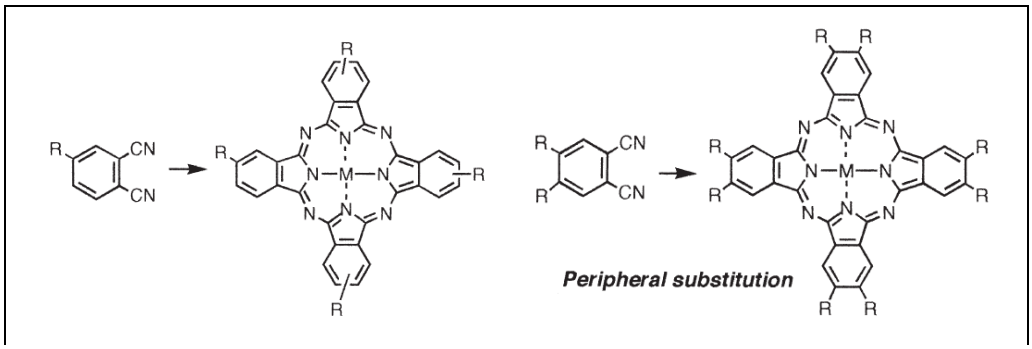

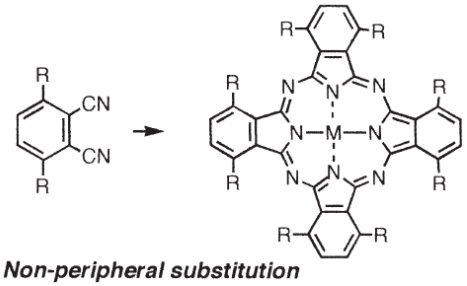

Fig. 1.2 Tetra and octa- substituted phthalocyanines and their phthalonitrile precursors

1.5 Molecular structure of H_2PcOC_8, $ZnPcOC_8$ and $CuPcOC_8$

It is well known that incorporating substituents onto the Pc ring is the most important method used to tune the physiochemical, electrochemical and spectroscopic properties of phthalocyanine derivatives. Thus far, various kinds of different substituents such as alkyl, alkoxy and thioalkoxy groups have been introduced onto the peripheral and / or nonperipheral positions of the Pc ligand [22]. Moreover, amongst the two possible peripheral octa-substitution patterns, that is the lateral positions (2, 3, 9, 10, 16, 17, 23, 24) and the radial ones (1, 4, 8, 11, 14, 15, 18, 22, 25) [23], the former have been commonly used one. In both cases columnar mesophases are formed, and result from the stacking of the flat and rigid phthalocyanine cores into columns, which are themselves arranged into a two dimensional lattice. The melting of the flexible side chains is responsible for the transition from the solid state to the liquid crystalline phase, while the aromatic cores retain some degree of the crystalline positional and orientational order. Because of their large conjugated molecular structure, together with strong π- π interactions between aromatic rings, Pc derivatives have also been used as sample building blocks for ordered molecular system [24]. Octakis (octyloxy)

substituted Pcs show self assembling [25]. Through self assembling process, functional molecules can self- assemble into a well defined monolayer with various patterns. By accurately controlling the self assembled monolayer, electronic devices can be developed.

1.5.1 2, 3, 9, 10, 16, 17, 23, 24 Octakis (octyloxy) Phthalocyanine (H_2PcOC_8)

Figure 1.3 shows the molecular structure of 2, 3, 9, 10, 16, 17, 23, 24 Octakis (octyloxy) Phthalocyanine. The molecular formula is $C_{96}H_{146}N_8O_8$ and its molecular weight is 1540.24.

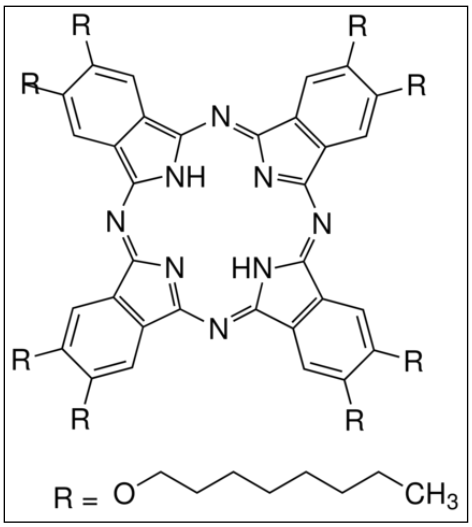

Fig. 1.3 The molecular structure of 2, 3, 9, 10, 16, 17, 23, 24 Octakis (octyloxy) Phthalocyanine

Properties

Material	**Physical properties**	**Uses**
2, 3, 9, 10, 16, 17, 23, 24 Octakis (octyloxy) Phthalocyanine	Colour -Dark blue Melting point>300 °C UV Absorption	Infrared Dyes, in organic and printed electronics, for photonic and optical materials

	maximum- λ_{max} 701 nm	

1.5.2 2, 3, 9, 10, 16, 17, 23, 24 Zinc Octakis (octyloxy) Phthalocyanine ($ZnPcOC_8$)

Figure 1.4 shows the molecular structure of 2, 3, 9, 10, 16, 17, 23, 24 Zinc Octakis (octyloxy) Phthalocyanine. The molecular formula is $C_{96}H_{144}N_8O_8Zn$ and its molecular weight is 1603.61.

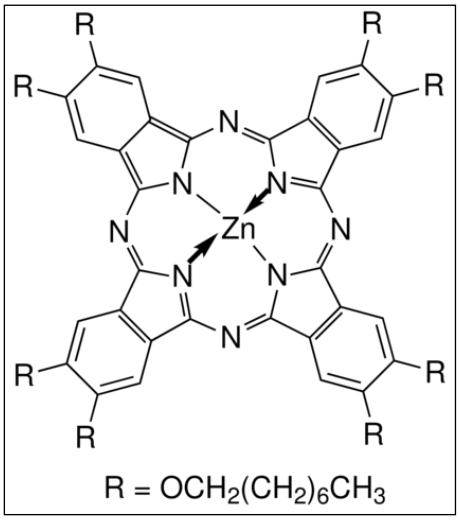

Fig. 1.4 The molecular structure of 2, 3, 9, 10, 16, 17, 23, 24 Zinc Octakis (octyloxy) Phthalocyanine

Properties

Material	**Physical properties**	**Uses**
2, 3, 9, 10, 16, 17, 23, 24 Zinc octakis (octyloxy) phthalocyanine	Colour-Dark blue Melting point>300 °C UV Absorption maximum- λ_{max} 677 nm	Infrared Dyes, in organic and printed electronics, for photonic and optical materials

1.6.3 2 ,3, 9, 10, 16, 17, 23, 24 Copper Octakis (octyloxy) Phthalocyanine ($CuPcOC_8$)

Figure 1.5 shows the molecular structure of 2, 3, 9, 10, 16, 17, 23, 24 Copper Octakis (octyloxy) Phthalocyanine. The molecular formula is $C_{96}H_{144}N_8O_8Cu$ and its molecular weight is 1601.7.

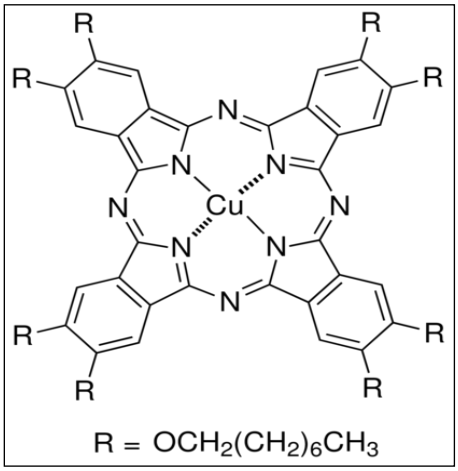

Fig. 1.5 The molecular structure of 2, 3, 9, 10, 16, 17, 23, 24 Copper Octakis (octyloxy) Phthalocyanine

Properties

Material	**Physical properties**	**Uses**
2, 3, 9, 10, 16, 17, 23, 24 Copper Octakis (octyloxy) Phthalocyanine	Dark blue colour Melting point>300 °C UV Absorption maximum- λ_{max} 677 nm	Infrared Dyes, in organic and printed electronics, for photonic and optical materials

1.6 Earlier studies on substituted phthalocyanine thin films

The structure of un- substituted Pc has been determined by Robertson et al. [26- 29]. The incorporation of long aliphatic chains as substituents in both octa- substituted series has received considerable attention in 1980s. These long chains enhance solubility in organic solvents and also promote

columnar liquid crystal behaviour. The latter discovery, with the first examples reported in 1982 [30], has significantly extended the range of so called discotic crystals [31], a class first identified by Chandrasekhar et al. in 1977 [32]. Groups led by Simon et al. [33- 34] and Notle et al. [35] in particular established that alkoxymethyl [30], alkoxy and alkyl chains [33-35] attached to the Pc nucleus at the peripheral sites lead to mesophase formation. During the same period, liquid crystallinity within the corresponding nonperipherally substituted compound was investigated by the group at the University of East Anglia (UAE). Mesophases are exhibited by the octa- alkyl [36] and octa- alkoxymethyl [37] series but not by the octa-alkoxy compounds [38]. Although there are many reports on MPcs with peripheral substituent groups [39], only a few studies on the introduction of octyloxy groups have been reported [40- 44]. But few data is available on the optical, electrical properties of H_2PcOC_8, $ZnPcOC_8$, and $CuPcOC_8$ thin films. Thus we have selected these materials in the present study. By knowing these properties and how the chain length of the substituted group affects them is very important for the fabrication of devices.

Wang et al. [44] did the density functional calculations for $CuPcOC_8$. The calculations show that for $CuPcOC_8$, both the in- plane interaction and stacking interaction are very strong and thus molecules could form continuous films. The gas sensing properties of the Langumir- Blodgett [LB] films of $CuPcOC_8$ in ethanol, methanol and propanol gases are reported by Jie et al. [45]. They found that the absorption spectra consist of two peaks in the visible region. Duan et al. [46] reported that alkoxy substituted PbPc complexes are used to obtain the optical limiting materials with broad protective wavelength and high optical transmission as well as quick response. Tunel et al. [47] studied the thermally induced molecular reorganisation within

the peripherally substituted PbPcs. Shirai et al. [48] reported on some properties of octathenyl- substituted Pcs prepared from the corresponding phthalonitrile obtained by the use of Suzuki- Coupling reaction between thiophene- 2- boronic acid and 4, 5 dibromophthalonitrile.

Fanli et al. [49] investigated the Raman spectroscopic characteristics of octa substituted bis (phthalocyaninato) rare earth complexes peripherally substituted with (4- methoxy) phenoxy derivatives. They reported that the introduction of substituted groups onto the phthalocyanine ring does not induce significant changes in the resonance Raman spectra. Wang et al. [44] observed highly homogeneous bar- shaped phthalocyanine aggregates with large aspects ratios are obtained by tuning of alkoxy substitutions in $CuPcOC_8$. Wang et al. [50] determined the crystal structure of the metal free 1, 4, 8, 11, 15, 18, 22, 25 octa- butyloxyphthalocyanine. They found that the crystal is of triclinic, space group $p\bar{1}$ with a = 14.0780 Å, b = 14.3480 Å, c = 17.0090 Å. In the crystal lattice, molecules overlap to each other with π- π interaction but the extent of overlap is different along the three axial directions. Vapour sensing properties of spin coated films of mesogenic octa substituted phthalocyanine derivatives ($MPcR_8$) have been investigated by Basova et al. [51]. The adsorption mechanism of chloroform and benzene vapours on gold coated glass slides is also studied. They found that the photodetector response is influenced by the substituents on the ring. Shaposhnikov et al. [25] have studied many specificities of bifunctional octasubstituted phthalocyanines by analysing their electronic absorption spectra, thermal stability. The analysis reveals that the electronic absorption spectra show that the introduction of peripheral substituents into the phthalocyanine strongly affects the absorption pattern. Tetra- 4- bromo-tetra- 5 (4- undecyloxybenzoylamino) and tetra- 4- phenoxy- tetra- 5- (4-

undecyloxybenzoylamino) phthalocyanine complexes of cobalt turned out to be light sensitive substances which may be used as materials for optical recording devices, including those operating in the IR region [52]. Bromo- and sulfo- substituted phthalocyanine copper complex has been tested as direct dye. The complex is greenish blue and its technical parameters are comparable with those of known copper (II) phthalocyaninetetrasulfonic acid tetrasodium salt [53]. The sensing layers of 2, 3, 9, 10, 16, 17, 23, 24- octakis (octyloxy) – phthalocyaninato complexes, $PcM(OR)_8$, with varying central atoms can be used for mass- sensitive transducer principles, as realized in microbalances such as cantilevers [54- 55] or quart- crystal microbalances (QCMs) [56].

Durmus et al. [57] have studied the photophysical and photochemical properties of tetra- and- octa- [4- (benzyloxy phenoxy)] substituted gallium (III) and Indium (III) phthalocyanines. They also have reported that the gallium and indium complexes show phototransformation during laser irradiation due to ring reduction. These complexes show potential as photodynamic therapy of cancer. Ray et al. [58] have used the ellipsometry and optical spectroscopy in the UV- Vis- NIR range to study the correlation between structure and optical properties of LB films of octa substituted metal free phthalocyanines containing different alkyl chains. They show that small changes in the alkyl length lead to significant changes in the Q- band shape. The spectral, photophysical and photochemical properties of tetra- and- octa carboxy substituted metallophthalocyanines containing silicon and germanium as central atoms have been studied by Idower et al. [59]. Surface Plasmon resonance of spun films of crown– ether substituted phthalocyanines and octa- 3, 7, 11- trimethyldodecycloxy phthalocyanine shows changes on exposure of the films to NO_2 [60]. Using Scanning

Tunneling Microscopy (STM) and XRD, Lei et al. [61] investigated the assembling behaviour of substituted phthalocyanines and porphyrins on both hydrophobic and hydrophilic surfaces. They show that $CuPcOC_8$ and 21, 23-dihydro- 5, 10, 15, 20- tetrakis [4- (tetradecycloxy) phenyl] porphyrin [TTPP] molecules adsorb stably on a highly oriented pyrolitic graphite (HOPG) surface, yielding high- resolution STM images. The results illustrate that alkyl molecular anchors can be used as generalized approach for immobilization of organic molecules on hydrophobic surfaces.

Wrobel et al. [62] have studied the influence of substituted different peripheral groups to ZnPc core and the correlation between the molecular structure and effectiveness of solar electric energy conversions. Haug et al. [63] have reported the investigations of vibrational properties of thin films in the dependence of the chain lengths on alkyl substituents in Pcs using total reflection- Fourier transform infrared spectroscopy, whereas the alkyl chains are C_4H_7, C_7H_{13}, $C_{10}H_{19}$. Fili et al. [64] have synthesised a new octa-cationic ZnPc, which is water soluble, but not aggregated under a wide range of solvent conditions, which is a power photosensitizer for the inactivation of microorganisms by using a strategy based on photodynamic therapy. Metal free and metallophthalocynines (M = Zn, Ni, ClFe) carrying eight hydroxyethylsulfanyl groups at the peripheral positions show more solubility in $CHCl_3$ due to esterification [65]. Hassan et al. [66] show that thin films of NiPc derivatives ($NiPcR_8$) with two different substituents R= $NHSO_2(C_6H_4)CH_3$, and $CH_2N(SO_2C_6H_4\text{-}CH_3)CH_2(CH_2)_8CH_3$ can be used as active layers of optical sensors for the detection of simazinc in water. Ceyhan et al. [67] have found that Four tert- Butylcalix [4] arene bridged double decker Lutetium (III) and Indium (III) phthalocyanines exhibit nonlinear optical limiting behaviour. Sugimori et al. [68] prepared and characterized 2,

3, 9, 10, 16, 17, 23, 24- octa substituted phthalocyanines modified with phenyl, tolyl, tert- butylphenyl and trifluoromethylphenyl groups. A number of unsymmetrically substituted Pcs and crown ether substituted Pcs have shown to form thermotropic liquid crystals [69]. The attachement of polar side chains such as oligo- (ethylene oxide) moieties and crown ether rings to large aromatic macrocycles is used in the construction of supramolecular wires and ion conducting channels [70]. In order to investigate the influence of chain length on mesophase behaviour, Sleven et al. [71] have prepared a series of homologous peripherally octa alkoxy substituted phthalocyanines. Ozcesmeci et al. [72] have proposed films of that metallophthalocyanines substituted with four pentafluoro benzyloxy units can be used as optical windows between the regions 400- 600 nm due to very low absorbances. The surface morphology of these films shows that molecules grow in stacks of rows rather in the zig- zag or parallel. Nombona et al. [73] have reported on the synthesis of unsymmetrically substituted magnesium phthalocyanine complexes containing one carboxyl group. The absorption spectra show a large split in the Q- band. These molecules can distinctly be employed in the field of photodynamic therapy in combination with fluorescence imaging.

Langumir- Blodgett deposits of the axial substituted cis- bis- decanoate- tin phthalocyanine on mica suggest that a combination of π- π, σ- π and Van der Waal's interactions are the leading factors for the deposition and for the control of supramolecular order [74]. The ultrafast dynamics of two Zinc (II) phthalocyanine derivatives with potential applications in photodynamic therapy has been studied by Fita et al. [75] using femto second transient absorption spectroscopy. The presence of long ester- alkoxy substituents at non- peripheral positions of the molecule leads to the slowdown of the thermalization of the molecules and shortens the excited-

state life time by a factor of approximately 3. Dincer et al. [76] analysed the symmetrical and unsymmetrical phthalocyanine macrocycles using spectroscopic methods including HNMR, electronic absorption, IR and mass spectroscopy. Their narrow long wavelength absorption band shows that bulky substituents on the periphery prevent aggregation. Achar et al. [77] have studied electrical conductivity of the symmetrical nickel (II) 2, 9, 16, 23- tetrahalo- substituted phthalocyanine complexes. They show that conductivity depends on the nature of the substituents and found to show ~10^3 times improved conductivity in comparison to parent nickel phthalocyanine complex. The substitution and iodine doping show remarkably high increased electrical conductivity in comparison to nickel phthalocyanine. Third order optical non linearities and optical limiting of octa- octyloxy phthalocyanine free base in toluene is analysed by Yu et al. [78]. The results suggest that octa- octyloxy Pc free base is promising for optical limiting materials. The optical limiting property of naphthalocyanine Zinc in DMSO solution has been first studied by Chunying et al. [79] with 30 ps laser pulses at a wavelength of 532 nm. Ma et al. [80] has investigated non linear optical properties of phenoxy- phthalocyanine and phenoxy- phthalocyanine zinc at a wavelength of 8000 nm with 100 fs pulses. The non linear absorption coefficient and non linear refractive index are measured using standard Z- scan technique. On alumina substrates, both CuPc and CuTTBPc thin films exhibit fine grain morphology and low crystalline structures. When the film is exposed to various concentrations of NO_2, a higher NO_2 concentration will lead to a lower film resistance which implies the possibility for the quantitative analysis of NO_2 concentration by these film sensors [81]. Absorption and fluorescence spectra of tetra- and – octa glycosylated ZnPc substituted with glucose and galactose has been analysed by Iqbal et al. [82]. Absorption

spectra showed a significant red shift in their Q- band maxima. Almari et al. [83] have prepared metal free 1, 4, 8, 11, 15, 18, 22, 25- octahexylphthalocyanine and thin films of the material are deposited on glass substrates by thermal evaporation technique. The structure of the film has been found to be in the α- form and shows strong peak indicating preferential orientation. Schuster et al. [84] investigated the effects of substrate temperature on the structural and morphological features of both cobalt phthalocyanine and cobalt hexadecafluorophthalocyanine thin films. Highly non aggregating hexadeca substituted phthalocyanine complexes are prepared by Mana et al. [85] and their fluorescence and non linear optical properties have been studied. They observe that such materials show non- aggregation behaviour, high solubility and red shifted Q- band, make such new chromophore materials to be attractive candidate for several applications such as PDT as photosensitiser, optoelectronics, and optical limiters and near- IR devices. Placing phenoxy groups at the nonperipheral positions of the phthalocyanine ring results in a shift of the Q- band in the visible spectrum into the near- IR region so that Pc does not play its characteristic blue or green colour [86].

The choice of octa substituted materials like H_2PcOC_8, $ZnPcOC_8$ and $CuPcOC_8$ are adequate for thin film fabrications on present outlook due to the following reasons. The novelty of those classes of materials is so clear from the review papers since they are very few in numbers. Though there are early reports of their optical applications, the electrical studies both in high and low temperature region are rare. Lack of available data in the structure and surface morphology of those materials still exists as a hindrance in their applications for constructing single molecular devices and in nano technological applications. A modest attempt has been made to study

electrical, optical, structural and surface morphological properties of H_2PcOC_8, $ZnPcOC_8$ and $CuPcOC_8$ materials by varying parameters like thickness, post deposition annealing temperature and irradiation of gamma rays.

References

1. Siegel R.W., Hu E.H., Roco M.C., WTEC Panel Report on R & D Status and Trends in Nanoparticles, Nano structured Materials and Nanodevices, Workshop 1997 (http://itri.loyola.edu/nano/ us_r_n_d/ toc.htm).
2. Kumar A., Chung Y.W., Moore J.J., Smugeresky J.E., Surface Engineering, Science and Technology I, The Minerals, Metals & Materials Society, Warrendale, 1999.
3. Kumar A., Chung Y.W., Chia R.W.J., Hard Coatings, The Minerals, Metals & Materials Society, Warrendale, 1998.
4. Leznoff C.C., Lever A.B.P, Eds.; Phthalocyanines: Properties and Applications, Vols. 1- 4; VCH Publishers: New York, 1989, 1993, 1996.
5. Hanack M.M., Heckmann H., Polley R., In Methods in Organic Chemistry (Houben- Weyl), Vol. 9 Eds, 1997.
6. Mc Keown N.B., Phthalocyanine Materials: Synthesis, Structure and Function; Cambridge University Press; Cambridge, 1998.
7. Moser F.H., Thomas A.L., The Phthalocyanines, Vols 1- 2, Manufacture and Applications; CRC Press; Boca Raton, 1983.
8. Gregory P., High- Technology Applications of Organic Colorants; Plenum Press: New York, 1991.
9. Gregory P., J. Porphyrins Phthalocyanines **4**, 432, 2000.
10. Ao.R, Kilmmert L., Haarer D., Adv. Mater., **7**, 495, 1995.
11. Brikett D., Chem. Ind, **4**, 178, 2000.

12. Worhle D., Meissner D., Adv. Mater., **3**, 129, 1991.

13. Eichhhorn. H., J. Porphyrins Phthalocyanines, **4**, 88, 2000.

14. Wright J.D., Prog. Sur. Sci., **1**, 31, 1989.

15. Snow A.W., Barger W.R., In Phthalocyanines- Properties and Applications; Leznoff C.C., Lever A.B.P, Eds.; VCH publishers: New York, 1989, p 341.

16. Nalwa H.S., Shrik J.S., In Phthalocyanines- Properties and Applications Vol. 4; Leznoff C.C, Lever A.B.P, Eds.; VCH publishers: New York, 1996, p 79.

17. Shrik J.S., Pong R.G.S, Flom S.R., Heckmann H., Hanack M., J. Phys. Chem., **104**, 1438, 2000.

18. de la Torre G., Vazquez P., Agullo Lopez, F. Torres, J. Mater Chem., **8**, 1671, 1998.

19. Luk'yanets E.A., J. Porphyrins Phthalocyanines., **3,** 424, 1999.

20. Hasrat H., Van. Lier, J.E. Chem. Rev., **99**, 2379, 1999.

21 . Priola S.A., Raines A, Caughey W.S., Science, **287**, 1503, 2000.

22. Xueying wang, Yuexing Zhang, Xuan Sun, Inorg. Chem., **46**, 7136, 2007.

23. Cammidge A. N, Cook M. J., Harrison K .J., Mc Keown N.B, J.Chem Soci. Perkin Trans., **5**, 3051, 1991.

24. Wang X., Chen Y., Lin H., Jiang J., Thin Solid Films, **496**, 619, 2006.

25. Shaposhmkov G.P., Maizlish V.E., Kulinich V.P., Russ J. Gen. Chem., **77,** 138, 2007.

26. Robertson J.M., J. Chem. Soc., **50**, 615, 1935.

27. Robertson J.M., J. Chem. Soc., **26**, 1195, 1936.

28. Robertson J.M., Woodward I, J. Chem. Soc., **22**, 219, 1937.

29. Robertson J.M., Woodward. I, J. Chem. Soc., **40**, 36, 1940.

30. Piechocki C., Simon J., Skoulios D., Guilon D., Weber P., J. Am. Chem. Soc., **104**, 5245, 1982.

31. Simon J., Bassoul. P., In Phthalocyanines- Properties and Applications, Vol.2; Leznoff C.C.; Lever A.B.P., Eds.; VCH publishers: New York 1996.

32. Chandrasekhar S., Sadashiva B.K., Suresh K.A., Pramana, **9**,471,1977.

33. Ohta K., Jaquemin L., Sirilin C., Bosio L., Simon J., New J. Chem., **12**, 75 1988.

34. Masural D., Sirilin C., Simon J., New J. Chem., **11**,455, 1987.

35. Van der Pol J.F., Neelmann E., Zwikker J. W., Nolte R.J.M., Drenth W, Recl. Trav Chim Pays-Bas, **107**, 615, 1988.

36. Cook M.J., Daniel M.F., Harrison K.J., McKeown N.B., Thomson A.J., J. Chem. Soc. Chem. Commun., **15**, 1086, 1987.

37. Cammidge A.N., Cook M.J., Haslam S.D., Richardson R.M., Harrison K.J., Liq. Cryst., **14**, 1847, 1993.

38. Cook M.J., Dunn A.J., Howe S. D., Thomson A.J., Harrison K.J., J. Chem. Soc. Perkin Trans, **1**, 2453, 1987.

39. Leznoff C.C. in Leznoff C.C., A.B.P. Lever (Eds), Phthalocyanines: Properties and Applications, VCH , New York, 1989(chapter1).

40. Chenjuan He, Yu Chen, Yuxin Nie, Duoyuan Wang, Optics Communications, **271**, 253, 2007.

41. Yu- Hong Liu, Shu- Xia Yin, Chi- Chiu Ma, Guan- Hua Chen, Chen Wang, Li- Jun Wan, Chun- Li Bai, Surf Sci., **559**, 46, 2004.

42. Zlatkin A., Yudin S., Simon J., Hanack M., Lehman H., Advanced Materials for Optics and Electronics, **5**, 259, 1995.

43. Meryen Camur, Mustafa Bulut, Dyes and Pigments, **77**,165, 2008.

44. Ming Wang, Yan- Lian Yang, Ke Deng, Chen Wang, Chem. Phys. Lett., **439**, 76, 2007.

45. Zhao Jie, Huo Li- Hua, Gao Shasn, Zhao Hui, Zhao Jing- Gui, Li Ning, Sensors and Actuators, **126**, 588, 2007.

46. Duan Q., Xia H., Liu D., Wang F., Toshifumi S., Toyoji K., Pb.Proc.SPIE. Int.Soc.Opt.Eng., **6028**, 602819, 2005.

47. Sinem Tuncel, Tamara .V. Basova, Vitaly.G. Kiselev, J. Mater. Res., **26**, 2962, 2011.

48. Shirai H., Muto T., Temma T., Kimura M., Hanabusa K., Chem. Commun., **21**, 1649, 2000.

49. Fanli Lu, Wendong Wang, Guihong Bao, Jianzhong Cui, Vibrational Spectroscopy, **56**, 228, 2011.

50. Wang Jun- Dong, Huang Jin- Ling, Cal Jin- Wan, Chen Nai- Sheng, Chinese. J. Struct. Chem., **21**, 617, 20002.

51. Basova T., Kol'tsov E., Ray A.K., Hasan A.K., Gurek A.G., Ahsen V., Sensors and Actuators B , **113**, 127, 2006.

52. Shaposhmkov G.P., Maizlish V.E., Kulinich V.P., Russ J. Gen. Chem., **74**, 395, 2004.

53. Lutensko O.G., Kulinich V.P., Shaposhmkov G.P., Arakcheeva A.A., Ru Patent 2233281, Byull. Lzobret, 2004, no.21.

54. Maute M., Raible S., Prins F.E., Kern D.P., Ulmer H., Weimar U., Gopel W., Sensors and Actuators B, **58**, 505, 1999.

55. Kim B.H., Maute M., Prins F.E., Kern D.P., Croitru M., Raible S., Weimar U., Gopel W., Microelectron Eng., **53**, 229, 2000.

56. Fietzek C., Bodenhoffer K., Haisch P., Hees M., Hanack M., Gopelm W., Sensors and Actuators B, **65**, 85, 2000.

57. Mahamut Durmus, Tebello Nyokong, Polyhedron, **26**,3323,20007.

58. Nabok A.V., Ray A.K., Hassan A. K., Travis J.R., Cook M.J., Supramolecular Science, **4**,407,1997.

59. Mopeloloa Idowu, Tebello Nyokong, J. Photochem. Photobiol. A. Chem., **204**, 63, 2009.

60. John D. Wright, Arielle Cado, Stanley J. Peacock, Vincent Rivalle, Ann M. Smith, Sensors and Actuators B, **29**, 108, 1995.

61. Lei S. B., Wang J., Dong Y.H., Wang C., Wan L.J., Surf. Interface Anal., **34**, 767, 2002.

62. Danuta Wrobel, Andrzej Boguta ,J. Photochem. Photobiol. A. Chem., **150**, 67, 2002.

63. Haug A., Harbeck S., Dini D., Hanack M., Cook M.J., Peisert H., Chasse T., Appl . Surf. Sci., **252**, 139, 2005.

64. Maria Paola De Filippis, Donata Dei, Lia Fantetti, Gabrio Roncucci, Tetrahedron Letters, **41**, 9143, 2000.

65. Barbaros Akkurt, Esin Hamuryudan, Dyes and Pigments, **79**, 153, 2008.

66. Assel Hassan, Tamara Basova, faltma Yuksel, Gulay Gumus, Ayse Gul Gurek,Uefa Ahsen, Sensors and Actuators B, Article in Press, doi.10.1026/jnsb 2011.12.029.

67. Tanju Ceyhan, Bekir Salib, Macroheterocycles, **1**, 44, 2008.

68. Tamostu Sugimori, Masaharu Torikata, Jun Nojima, Inorg. Chem Comm., **5**, 1031, 2002.

69. Piechocki C., Simon J., J. Chem. Soc., **139**, 239, 1985.

70. Von Nostrum F., Picken S.J., Schouten A, J., Nolte R.J.M., J.Am. Chem. Soc., **117**, 9957, 1995.

71. Juegon Sleven, Christiane Goreller - Walrand, Koen Binnemanns, Mat. Sci. Eng:C., **18**, 229, 2001.

72. Mukaddes Ozcesmeci, Idris Sorar, Esin Hamuryudan, Synthetic Metals, **162**,154, 2012.

73. Nolwazi Nombona, Wadzanai Chidawamikya, J. Mol. Struct., **1012**,34,2012.

74. Jose Campos Teran, Cristina Garzai, Hiram I Beltran, Thin Solid Films, **520**, 2211, 2012.

75. Piotra Fita, Tomsz Osmalek, Tomasz Goslink, J. Photochem. Photobiol A. Chem., **2323**, 44, 2012.

76. Ahmet Lutfi Ugur, Hatice A Dincer, Ali Erdogmus, Polyhedron, **31**, 431, 2012.

77. Achar B.N., Jayasree P.K., Synthetic Metals, **114**, 219, 2000.

78. Chen Yu, Wang Duoyuan, Opt. Eng., **40**, 2683, 2001.

79. Chunying He, Wubiao Duan, Yiquan Wu, Proceeding of SPIE, **32**, 6595, 2007.

80. Lei Ma, Yundong Zhang, Ping Yuan, Optics Express, **18**, 17666, 2010.

81. Yuh–Lang Lei, Chuan Yi Hsiao, Chien–Hsiang Chang, Yu-Min Yang, Sensors and Actuators B. Chemical, **94**, 169, 2003.

82. Zafar Iqbal, Nkosiphile Masilela, Teberllo Nyokong, Photochem. Phtobiol . Sci., **11**, 679, 2012.

83. Almari S.N., Joraid A.A., Al- Raqa S.Y., Thin Solid Films, **510**, 265, 2006.

84. Britt-Elfriede Schuster, Tamara Basova, Keiko Peisert, Thomas Chasse, Thin Solid Films, **518**, 7161, 2010.

85. Hacene Manaa, Abdullah Al Mulla, Saad Maksheed, Moyyad Al-sawah, Jacob Samuel, Optical Materials, **32**,108, 2009.

86. Bhardwaj N., Andraos J., Leznoff C.C., Canadian J. Chem., **80**,141,2002.

CHAPTER 2

INSTRUMENTS AND EXPERIMENTAL TECHNIQUES

2.1 Introduction

Thin films play an important role in technological development and techniques of film deposition offer a major key to the fabrication of solid state microelectronic devices. Although there are many methods for depositing thin films, thermal evaporation technique has some advantages [1]. Deposition of thin films by thermal evaporation is very simple and convenient and is the most extensively used technique [2]. Phthalocyanines can be sublimed, resulting in materials of purity (10^{14}- 10^{16} traps per cm^3) exceptional in organic chemistry [3]. In vacuum most Pc complexes do not decompose below 900^{o}C. Therefore, thermal evaporation under high vacuum is used in this work to prepare stable and homogeneous thin films of H_2PcOC_8, $ZnPcOC_8$ and $CuPcOC_8$. Properties of phthalocyanine thin films strongly depend on the method of deposition, the substrate materials, and the

substrate temperature, the rate of deposition, post deposition heat treatment and background pressure [4-7]. The high vacuum environment and the well controlled growth conditions allow the production of high- quality thin film layers with an exceptional purity.

However the growth of organic thin films presents several problems inherently related to the nature of these relatively large molecules. First of all, the unit cells of these materials are large compared to those of the typical inorganic substrates and they exhibit a very low symmetry [8- 9]. In contrast to conventional inorganic semiconductor thin film growth, where the ad-molecules are usually single atoms with spherical symmetry, for organic semiconductors each ad- molecule can involve more than fifty atoms covalently bonded forming a unit with very low symmetry. The dimensions of these molecular units are in the nanometer scale and thus deposition on inorganic substrates presents lattice mismatches of one order of magnitude [10]. This frequently leads to the growth of films presenting multiple rotational and translational domains, since several energetically equivalent orientations of the organic lattice on the inorganic substrate exist. Secondly, the chemical nature of the substrate is crucial. Strongly interacting substrates usually limit the surface mobility of the molecules during film formation and thus leading to a high density of grains. Moreover, polymorphism is favoured by the weak intermolecular interactions responsible for the crystal packing. In conclusion the presence of several azimuthal domains, small grain size and coexistence of different polymorphic forms are common in the growth of organic thin layers.

2.2 Methods of preparation of thin films

A ‘thin film’ may be arbitrarily defined as a solid layer having a thickness varying from a few A^0 to about 10 μm. Since the thickness

limitation is rather arbitrary, even somewhat thicker films may also come within the scope of this definition. Whatever be the film thickness limit, an ideal film can mathematically defined as a homogeneous solid material contained between two parallel planes and extended infinity into two directions (x, y axis) but restricted along the third direction which is perpendicular to (x, y) plane [11]. A real film however deviates considerably from the ideal case since its two surfaces are never exactly parallel even when formed in the best experimental deposition conditions and also the material contained between the two surfaces are rarely homogenous. Thin films can be prepared from a variety of materials such as metals, semiconductors, insulator or dielectric and for this purpose various preparation techniques are developed [11- 12].

The general methods of preparation of thin film may be classified into these groups.

1. Physical methods
2. Chemical methods
3. Sputtering

Each of the above mentioned methods has its own advantages and disadvantages and our discussion restricts only on thermal evaporation method which we have used to prepare the films in the present study.

2.3 Physical vapour deposition - Thermal evaporation

The deposition by thermal evaporation method is simple, very convenient and at present it is the most widely used technique [13]. This method uses high temperature to sublimate the source material into vapour state. The atom or molecule of the source is speeded up by high temperature passing through a vacuum space, condensing of a vapourised form to

substrate surfaces. The vacuum is required to allow the molecules to evaporate freely in the chamber, and they subsequently condense on the substrate surfaces. As the term "Thermal" indicated, the thermal high temperature is the key role of this method. "Thermal High Temperature" is same for all evaporation technologies, only the techniques used to the heat the source material differs. Several techniques are used to obtain the high temperature. Here we have employed resistive heating technique in high vacuum.

In resistive heating, a big current passing through the resistor (the source material is put or attached on the resistor), the resistor will generate high temperature and sublime the target material. Traditionally the resistors are made by W (Tm=3380℃), Ta (Tm=2980℃), Mo (Tm=2630℃) which have very high melting temperatures. The melting temperature of source material is much lower than that of resistors. When the current passes, only the source material get melted or vapourised and "fly" to the substrate surface. The resistor can be made of different shapes depending on what amount of the source material one wants to evaporate and the uniformity of evaporation. The wire (filament) is first to be used as resistor and attached with targets (Al, Ag, Au, Cr...).

This method has the following advantages:

1. Impurity concentration in the film is minimum.
2. Material boils at lower temperature under vacuum.
3. Growth can be effectively controlled.
4. Mean free path of the vapour atom is considerably larger at low pressure and hence a sharp pattern of the film is obtained.

5. A large number of materials can be used as substrate.

The evaporation rate and hence the condensation have wide limits, depending upon the purity of source material used. Characteristics of the prepared films are determined by parameters such as temperature, type of substrate, deposition rate and residual atmosphere. All these parameters can be controlled in thermal evaporation method. Also single evaporation can give films of different thicknesses. We have used here molybdenum boats and tungsten baskets for evaporation of materials. Films of high purity can readily be produced with a minimum of interfering conditions.

2.4 Vacuum coating unit

The type of vacuum equipment needed depends on the desired purity of the film. The vacuum system employed to deposit and characterize thin films in the present work contains an assortment of pumps, tubings, valves and gauges to establish and measure the required pressure as shown in Figure 2.1. Basically the vacuum system, "Hind Hivac" coating unit (Model No. 12A4) consists of 0.4 m diffusion pump in conjunction with an oil- sealed rotary pump. The ultimate pressure that can be achieved in a 0.3 m diameter stainless steel bell jar is of the order of 1.3×10^{-6} Pa. It has facilities for electron beam evaporation and flash evaporation. A low tension transformer (10V; 100 A) is used for heating the vapour source. Most of the evaporations are carried out at a pressure of 1.3×10^{-6} Pa. The pressure is measured by means of a Priani gauge and the diffusion pump vacuum is measured by a Penning gauge.

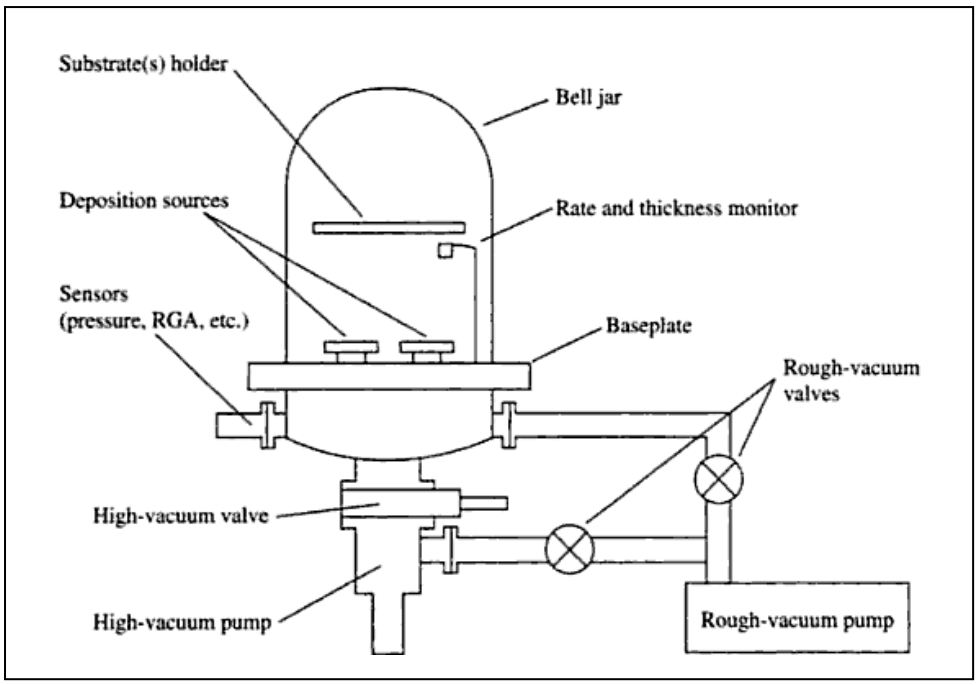

Fig. 2.1 Schematic representation of a typical vacuum system used for thin film deposition

The Pirani gauge (A6 STM) has two gauge heads, which facilitate the measurements of the fore vacuum and roughing vacuum. Change of pressure in the vacuum system brings about a change in the number of gas molecules present and hence a change in the thermal conductivity of the gas.

Thus the heat toss of the constant voltage electrically heated filament in the system varies with the pressure. The filament of the Pirani gauge head has high temperature coefficient of resistance. So a slight change in the system pressure brings about useful change in the filament resistance resulting in an out of balance current in the Wheatstone's bridge, which can be read as pressure on a meter as shown in Figure 2.2. The filament is often reconditioned if the gauge behaves erratically when it is filled with contaminants. For this the gauge head is flushed with acetone and thoroughly

dried 10 V d.c is applied across the filament to volatilize the deposits on the filament.

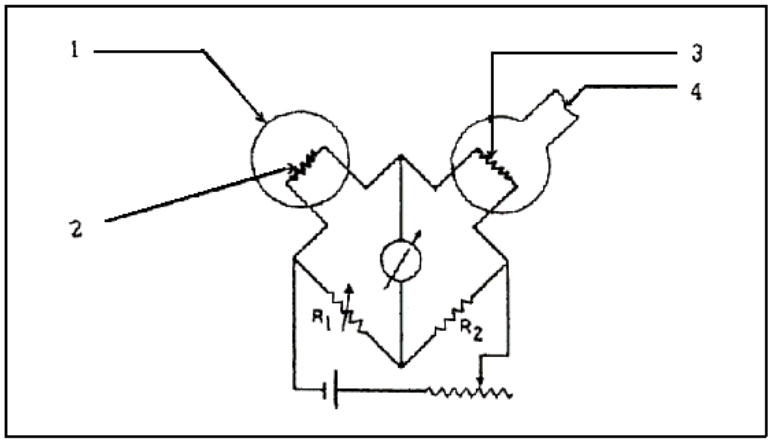

Fig. 2.2 Schematic representation of Pirani gauge

1. High Vacuum
2. Reference wire
3. Sensing wire
4. Vacuum system

The Penning gauge (STP4M – 1) is used to measure the vacuum in the range of 10^{-3} to 10^{-6} Pa, ie; two ranges with instant range changing provided by a toggle switch. This is a cold cathode ionization gauge head and consists of two electrodes, anode and cathode as given in Figure 2.3. A potential difference of about 2.3 kV is applied between anode and cathode through correct limiting resistor. A magnetic field is introduced at right angles to the plane of the electrodes by a permanent magnet having nearly 800 gauss, which will increase the ionization current. The electrons emitted from the cathode of the gauge head are deflected by means of the magnetic field and are made to take helical path before reaching the anode top. Thus following a long path, the chance to collision with gas molecules is high even at low pressures. This facilitates an increase in the number of secondary electrons. Eventually the electrons are captured by the anode and thereby providing an electron current through the

anode. This current is used as a measure of pressure of the gas. If the gauge shows unstable pressure reading due to the contamination of the gauge head by forming a thin layer of deposition on the anode loop and cathode liner, it is cleaned chemically by heating at 333 K for 20 minutes is a solution of 20- 30% HNO_3 and 2- 3% HF acids.

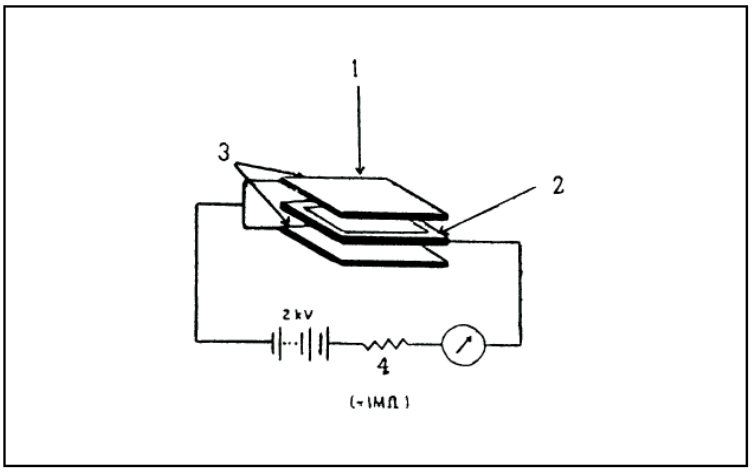

Fig. 2.3 Schematic representation of Penning gauge

1. Magnetic field
2. Anode (+)
3. Cathodes (-)
4. Ballast resistor

2.5 Preparation of films

Thermal evaporation method is used for the preparation of thin films. The films are deposited on to clear glass substrates. In thermal evaporation, the material is heated to vapour form by means of resistive heating. On heating the materials in vacuum, sublimation takes place and the atoms are transported and get deposited on to the cleaned substrates held at suitable distance. The material for deposition is supported onto a vapour source that is heated to produce desired vapour pressure. The requirements for the vapour source are that it should have a low vapour pressure at the deposition

temperature and should not react with the evaporant. We have used tungsten helical baskets and molybdenum boats as the vapour sources. The evaporant material in the powder form is kept in the molybdenum boat. The low tension (LT) supply (10 V; 100 A) for evaporation source is obtained from a step- down transformer. The LT output from the transformer is fed through a current meter and a selector switch to LT feedthrough and filament holders. A variable voltage transformer provided in the circuitry facilitates the precise control of current through the tungsten basket or molybdenum boat.

2.6 Substrate cleaning

For deposition of films, highly polished and thoroughly cleaned substrates are required. First the substrates are cleaned using liquid detergent. Then it is kept in dilute nitric acid. After this, they are cleaned using distilled water and agitated in acetone. They are then rinsed in isopropyl alcohol and dried in hot air. Subsequently the substrates are subjected to ionic bombardment for three minutes as final cleaning before deposition. The ions are produced by high- tension (HT) discharge.

2.7 Thickness measurement

There are different techniques to determine the film thickness [14-15]. We have used Tolansky's Multiple beam interference technique for the precise measurement of thickness of the film. This technique can be used to measure even ultra- thin films with an accuracy of ± 0.8 nm [15]. The schematic representation of the fringes produced by multiple beam interference is as shown in Figure 2.4.

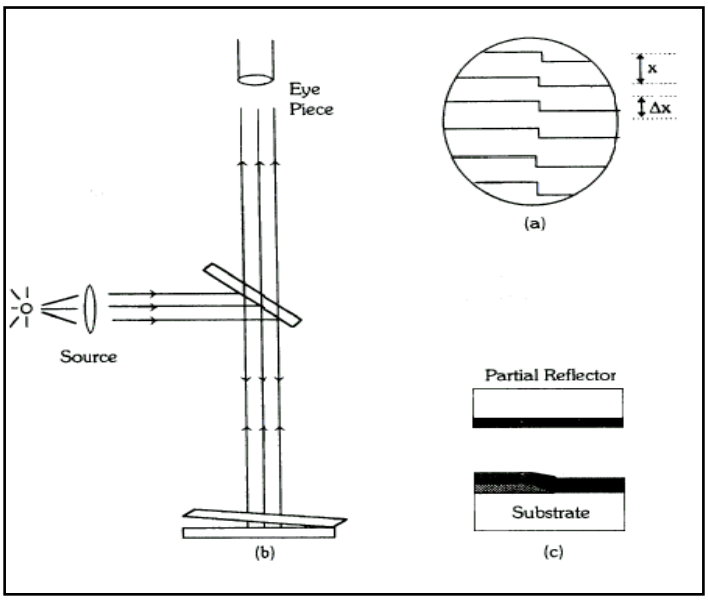

Fig. 2.4 Schematic representation of Multiple beam interference technique

This technique can be employed when the film to be studied remains stable in vacuum and can be coated with a high reflecting layer [15]. During the coating of the film, a sharp edge is produced by shadowing with sharp masks during deposition. The film is then coated with a highly reflecting silver layer. A second glass plate with a silver coated surface and having some percentage of transmission is lowered onto the glass substrate and the whole system is illuminated with a parallel beam of monochromatic light of wave length (λ = 5893 A^0) from a sodium vapour lamp. The semi- silvered glass and the substrate with the film on it are so positioned that an air wedge is formed in between them. Fringes of band width 'x' appear due to multiple beam interference. In the region of sharp edge, the fringes are shifted by a distance 'Δx' in x corresponding to a thickness step of $\lambda/2$. The thickness (t) of the film is determined as

$$t = \{[\Delta x]/x\}\ [\lambda/2] \qquad 2.6.1$$

2.8 Sample annealing

The samples are annealed in a specially designed furnace capable of producing a maximum of about 670 K. It consists of a coil of Kanthal (A1 grade temperature range 1150-1350 ^{0}C). To avoid heat loss, it is surrounded by a thick package of fire brick silica whose working temperature is 1100^{0}C and the melting point is 1710^{0}C. The width of the heating element is about 20 cm. The filament is also covered with sillmate ($Al_2 O_3 - Si O_2$) tube, maximum working temperature is 1500^0 C and melting point is 1710^{0}C. It helps to provide uniform heating region at the centre of the tube. In addition it avoids any thermal shock during the annealing process. The temperature of the heater is controlled and recorded by a digital temperature controller cum recorder.

2.9 Conductivity measurements

The electrical conductivity measurements are carried out in a conductivity cell. The schematic diagram of the conductivity cell is shown in Figure. 2.5. The cell consists of a thick walled cylindrical chamber with a bottom flange and four side tubes made of stainless steel. Three side tubes are closed air tight with glass windows and are used in spectroscopic studies. The remaining side tube is connected to a rotary vacuum pump and the chamber can be evacuated to low pressure of 10^{-3} mbar. The inner tube is made of stainless steel pipe which has been welded to a large copper finger. The liquid nitrogen cavity and the heated coil help the sample to attain the required temperature very quickly. The outer enclosure is made leak proof by using an 'O' ring which rests inside the groove on the flanges. A sample holder fixed at the copper finger can hold the film with the help of screws. The outer surface of the copper finger is covered with mica sheets and the heating coil is wound over it. The electrical leads are taken out through

Teflon insulation. A d.c power supply is used to heat the heater coil. The electrical leakage current through the mount is by- passed to earth by grounding the inner tube. The leads of the electrodes are taken out using BNC connector. A chromel- alumel thermocouple in contact with the sample senses the temperature. Temperature of the sample in the cell can be varied from liquid nitrogen temperature to 400^0C.

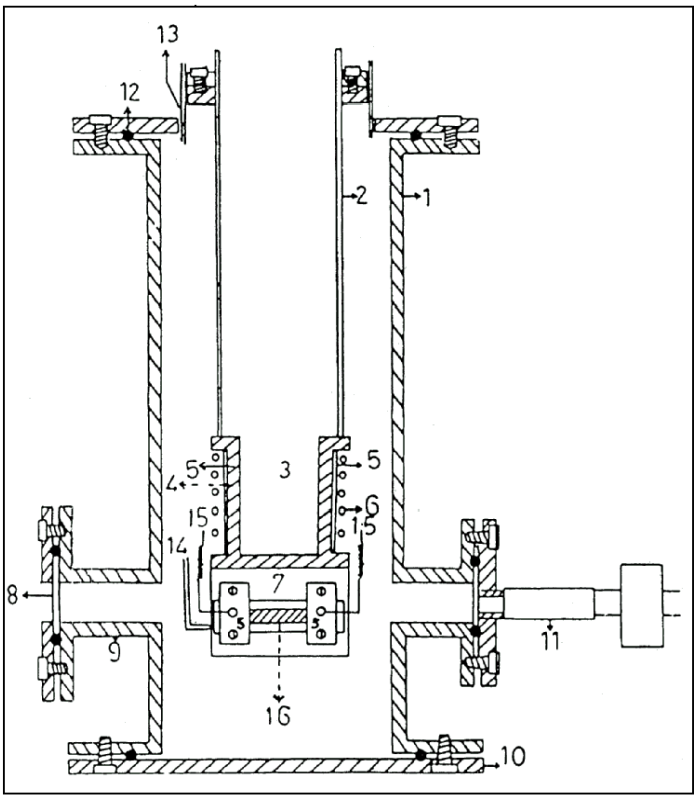

Fig. 2.5 Schematic diagram of the cross section of the conductivity cell

1. Cylindrical chamber
2. Inner tube
3. Liquid nitrogen cavity
4. Copper finger
5. Mica insulator
6. Heater coil
7. Sample holder
8. Glass window
9. Side tube
10. Bottom flange
11. Rotary pump
12. Neoprene “O” ring
13. BNC

14. Thermocouple
15. Connecting leads to BNC
16. Substrate with film

Electrical conductivity measurements are carried out using Keithley programmable electrometer model No. 617. It is a highly sensitive instrument designed to measure voltage, current, charge and resistance. The very high input resistance, low input offset current and sensitivity allows accurate measurements. The measuring range is in between 10 μν and 200 V for voltage measurements, 0.1 pA and 20 mA in the current mode and 10 fC and 20 nC in coulomb mode. The resistance can be measured in two modes. (1) constant current mode (2) constant voltage mode. Due to the high input resistance, a resistance as high as 200 GΩ can be measured in the constant current mode. Using constant voltage mode resistance as high as 10^6 Ω can be measured. In this mode the measured resistance is automatically calculated from the applied voltage. The model 617 has a built in voltage source which can be used to apply a current I, through the unknown resistance. The insulation resistance is then automatically calculated by the instrument as R=V/I, where I is the current through the resistance and V is the programmed voltage. The voltage can be programmed between -102. 35 V and +102.4 V in steps of 50 mV and the maximum measurable output current is 2 mA. The instrument is capable of an internal 100 point data store and that can be used to login a series of readings. The fill rate of date store can be set to specific intervals according to the experimental conditions.

2.10 UV- Visible Spectrophotometer

A diagram of the components of a typical spectrometer are shown in the Figure 2.6. The functioning of this instrument is relatively straightforward. A beam of light from a visible and/or UV light source (coloured red) is separated into its component wavelengths by a prism or diffraction grating. Each monochromatic (single wavelength) beam in turn is split into two equal intensity beams by a half- mirrored device. One beam, the sample beam (coloured magenta), passes through the film. The other beam, the reference (coloured blue), passes through an identical substrate. The intensities of these light beams are then measured by electronic detectors and compared. The intensity of the reference beam, which should have suffered little or no light absorption, is defined as $\mathbf{I_0}$. The intensity of the sample beam is defined as **I**. Over a short period of time, the spectrometer automatically scans all the component wavelengths in the manner described. The ultraviolet (UV) region scanned is normally from 200 to 400 nm, and the visible portion is from 400 to 800 nm.

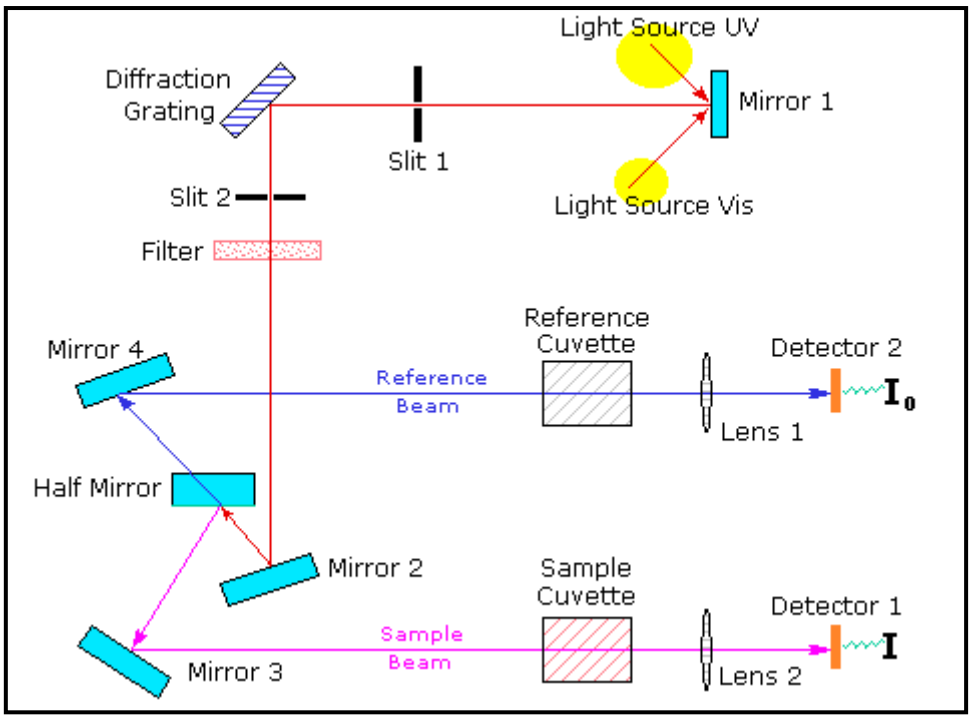

Fig. 2.6 Schematic representation of an UV- Visible Spectrophotometer

If the sample film does not absorb light of a given wavelength, $I = I_0$. However, if the sample film absorbs light then I is less than I_0, and this difference may be plotted on a graph versus wavelength. Absorption may be presented as transmittance ($T = I/I_0$) or absorbance ($A = \log I_0/I$). If no absorption has occurred, T = 1.0 and $A = 0$. Most spectrometers display absorbance on the vertical axis, and the commonly observed range is from 0 (100%

transmittance) to 2 (1% transmittance). The wavelength of maximum absorbance is a characteristic value, designated as λ_{max}.

2.11 Gamma ray chamber

Gamma ray chamber 5000 is a compact self- shielded Cobalt- 60 research irradiator providing an irradiation volume of approximately 5000 cc. The schematic representation of the Gamma ray chamber 5000 is shown in Figure 2.9. The material for irradiation is to be placed in a sample chamber located in Central Drawer of the unit. The drawer can be moved up and down with the help of a system of motorized drive and its associated mechanism which enable precise positioning of the sample Chamber at the centre of the radiation field inside the unit.

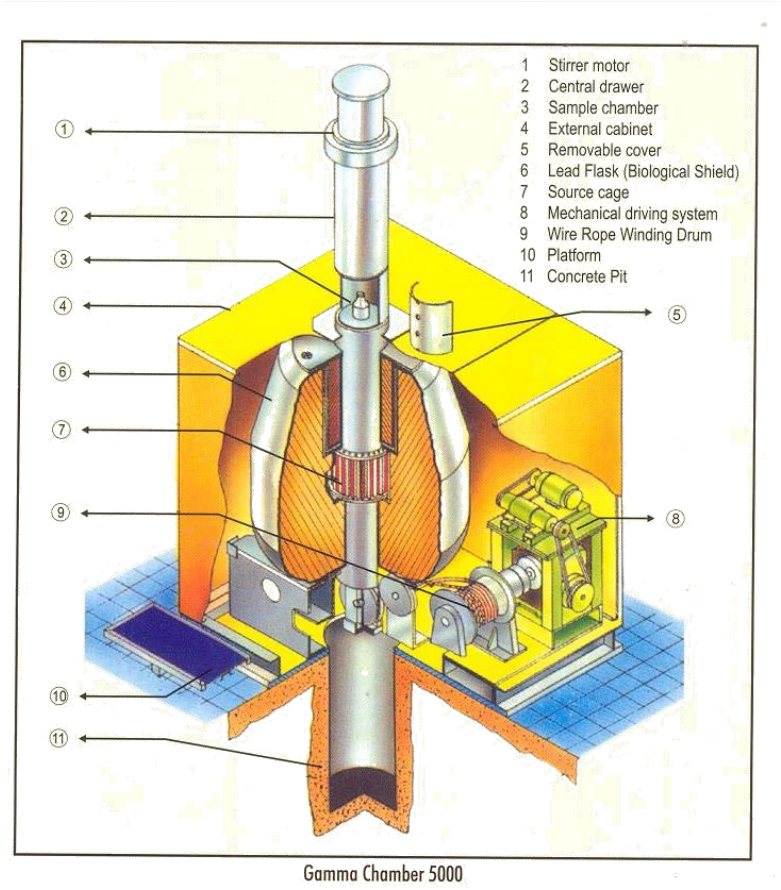

Fig. 2.7 Schematic representation of the Gamma ray chamber 5000

Radiation field is provided by a set of stationary Cobalt- 60 sources placed in a cylindrical cage inside the source lead flask through which the drawer moves up and down. The sources are doubly encapsulated in corrosion resistant and leak proof stainless steel pencils which are tested in accordance with international standards. Access holes of 8mm diameter are provided in the drawer for introduction of service sleeves for gases and thermocouple. A

mechanism for rotating/stirring samples during irradiation is also incorporated. The lead shield provided around the source is adequate to keep the external radiation field well within the permissible security limits.

References

1. Chopra K. L., Thin Film phenomena, MC-Graw Hills, New York, 1969.
2. Joy George, Preparation of thin films, Marcel Dekker, New York, 1992.
3. Simon J., Andre J.J., Molecular Semiconductors Photoelectrical properties and Solar cells, Springer Verlag, New York, 1985.
4. Riad A.S., Physica. B, **270**, 148, 1999.
5. Hsich J. C., Liu C. J., Ju Y.H., Thin Solid Films, **322**, 98, 1998.
6. Unni K. N. N., Menon C.S., J. Mater. Sci. Lett., **20**, 1207, 2001.
7. Hassan A.K., Gould R.D., J. Phys. Condens. Matter, **1**, 6679, 1989.
8. Umbach E., Sokolowski M., Fin'k R., Appl. Phys., **63**,565, 1996.
9. Hooks D.E., Fritz T., Ward M.D., Adv. Mater., **13**,227, 2001.
10. Forrest S.R., Chem. Rev., **97**, 1793, 1997.
11. Goswami A., Thin Film Fundamentals, New Age International (p) Ltd., New Delhi, Bangalore, 1982.
12. Holland L. Vacuum Preposition of Thin Films John Wiley, New York, 1956.
13. Glang R., Handbook of Thin Film Technology, Mc- Graw- Hill, New York, 1970.
14. Maissel L.I., Glang R., Hand Book of Thin Film Technology, Mc- Graw Hill Book Co; New York, 1983.
15. Ludmila Eckertova, Physics of Thin Films, II Eds, Plenum Publishing Corporation and SNTL, Prague 1990.

CHAPTER 3

EFFECT OF GAMMA RADIATION ON THE OPTICAL AND ELECTRICAL PROPERTIES OF H_2PcOC_8, $ZnPcOC_8$ AND $CuPcOC_8$ THIN FILMS

3.1 Introduction

The primary interactions between energetic radiation, semiconductors and inorganic insulators result in the loss of energy to their electrons, and this energy is ultimately converted to the form of electron-hole pairs. In this process, known as ionization, the valence band electrons in the solid are excited to the conduction band and are highly mobile, if an electric field is applied [1]. Thus, any solid irradiated with an energetic radiation conducts for a time at a higher level than normal. The production and subsequent trapping of the holes in oxide films cause serious alterations in the device's performance.

In organic materials under irradiation, a chain of reactions, in which oxygen and moisture from the environment may be incorporated, starts with rapid electronic phenomena. This is followed by the generation of reactive; short- lived intermediate compounds and a complex mixture of chemical products. The main result of ionization is the breaking of chemical bonds and the creation of new ones, which causes change in conductivity and leads to long- lived forms of physical breakdown. Changes in the electrical properties of metals under irradiation are considered mainly in nuclear reactor applications, where small conductivity alterations due to atom displacement might affect a carefully balanced microelectronic circuit [1]. Optical absorption analysis has widely proven to be an important and efficient tool in exploring and interpreting the various phenomena of electronic structures and processes in the materials subjected to radiation [2– 4]. The considerable theoretical investigations on the optical behaviour of thin films deal primarily with optical reflection, transmission, and adsorption properties, and their relation to the optical constants of films [2]. The importance of studying the optical properties of a material is offered by the ability of this technique to provide information regarding the fundamental gap, electronic transition, trapping levels, and localized states. In general, films are amorphous, and at most they are polycrystalline in nature. Over the last decades, advances have been made in understanding the problem of how the disorder in amorphous materials influences the band structure and hence the electrical and optical properties of the material. For semiconductors, the main characteristics of the energy distribution of electronic states density of the crystalline solids are the sharp structure in the valence and conduction bands, as well as the abrupt terminations at the valence band maximum and the conduction band minimum. The sharp edges in the density of states curves produce a well- defined forbidden energy gap. An amorphous solid is a material lacking any form of structural order. The amorphous state is to some extent unstable or meta- stable [5] and frequently exhibits a gradual or even rapid transition to an ordered crystalline condition. Despite the presence of high density disorder in amorphous

materials, they depart only slightly from the ideal crystalline structure [5]. In other words, short- range order can be assumed due to the rigidity of the chemical bonds, and the fundamentals of crystal band structure still holds for amorphous solids [6]. Nominally amorphous films may differ in their electrical and other properties according to the manner of their preparation. In particular, the deposition rate in evaporated films is known to have a profound influence on the dielectric constant and the level of conductivity [7].

The exposure of every solid material to ionizing radiations produces changes in the micro structural properties of the material, which in turn affects the optical, electrical and other physical properties of the material [8- 10]. Efforts are on world over to investigate the influence of gamma radiation on thin films and thin film structures of different metal oxides and polymers, in order to find out the suitability of using thin films and thin film structures of different metal oxides and polymers as post– exposure as well as real– time gamma radiation dosimeters [11- 17]. Naturally, a deep understanding of the physical properties of these thin films under the influence of gamma radiation is quite important from the view point of design of novel real– time gamma radiation dosimeters possessing high sensitivity. The effect of ionizing radiations depends on both the radiation dose and the parameters of the films including film thickness.

3.2 Theory

Cobalt is a hard, silvery- white metal that occurs in nature as cobalt- 59. Cobalt is a constituent of the minerals cobaltite, smaltite, erythrite and other ores, and it is usually found in association with nickel, silver, lead, copper, and iron. Pure cobalt metal is prepared by reducing its compounds with aluminium, carbon, or hydrogen. It is similar to iron and nickel in its physical properties. Cobalt has relatively low strength and little ductility at normal temperatures and is a component of several alloys.

Cobalt- 60 (^{60}Co) is a synthetic radioactive isotope of cobalt with a half- life of 5.27 years. It is produced artificially by neutron activation of the isotope ^{59}Co. ^{60}Co decays by beta decay to the stable isotope nickel-60 (^{60}Ni). The activated nickel nucleus emits two gamma rays with energies of 1.173 and 1.332 M eV, hence the overall nuclear equation of the reaction and the schematic representation of the decay is shown in Figure 6.1.

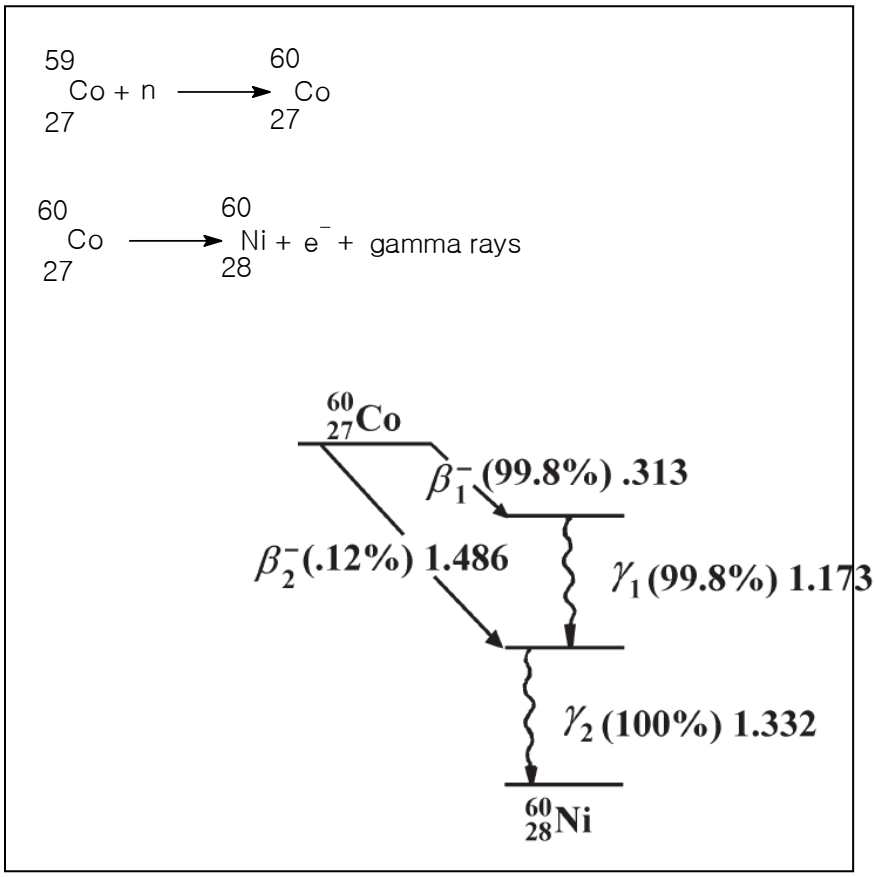

Fig. 3.1 Decay scheme of radionuclide cobalt- 60

3.3 Experiment

Employing thermal evaporation in vacuum as described in section 2.5 of chapter 2, thin films of H_2PcOC_8, $ZnPcOC_8$ and $CuPcOC_8$ of thickness 250 ± 5 nm are prepared on suitably cleaned glass substrates using Hind Hivac 12 A4 coating unit. Glass slides of dimensions 40 mm x 12 mm x 1.3 mm are used as substrates. The substrates are cleaned as stated in the procedure described in section 2.6 of chapter 2. Evaporation of the material is performed at a base pressure of 1.3 x 10^{-6} Pa from a molybdenum boat of dimensions 2.9 cm x 1.2 cm x 0.5 cm which is used as the resistive heating element. Thickness of the films is determined using the procedure described in section 2.7 of chapter 2. Thin films deposited at room temperature are further annealed in air at various temperatures. At room temperature, a disc– type ^{60}Co gamma radiation source was used to expose these thin films to various levels of gamma radiation dose. UV – Vis absorption and reflection spectra of the gamma irradiated H_2PcOC_8, $ZnPcOC_8$ and $CuPcOC_8$ thin films are recorded using the 'Shimadzu 160 A' Spectrophotometer. Electrical measurements are performed using a programmable Keithley electrometer (model No. 617) in the constant current source mode.

3.4 Results and Discussion

3.4.1 Optical properties

3.4.1.1 H_2PcOC_8 thin films

The optical absorption spectra of γ irradiated H_2PcOC_8 thin films of thickness 250 ± 5 nm for various radiation doses are shown Figure 6.2. As the γ radiation dose increases, the absorbance decreases. The spectra originate from the orbital within the aromatic 18 π – electron system. The electronic π- π^* transition in the energy range 300- 330 nm corresponds to an intense B- band (Soret band) which gives the fundamental absorption edge, while the band in the energy range 620- 697 nm (Q – band) gives the excitonic energy [18- 19]. The interaction between molecules strongly influences the absorption spectrum leading to splitting of Q- band into two distinct peaks. The fundamental absorption edge is analysed within the frame work of one electron theory of Bardeen et al. [20]. A satisfactory linear fit is obtained for α^2 versus hυ, indicating the presence of direct allowed transition. Figure 6.3 and 6.4 represents the α^2- hυ graphs of the H_2PcOC_8 thin films irradiated with different γ radiation dosages for the Q- band and B- band respectively. The intercept on the energy axis gives the excitonic and fundamental energy gap, which is collected in Table 6.1. As the radiation dosage increases, there is a slight decrease in the value of the excitonic and fundamental energy gap. But on γ irradiation, the band gap energy reduced from the as deposited value of 3.18 eV (Figure 4.6) to 3.14 eV. This is due to the fact that, the γ irradiation brings about disorder within the film matrix by inducing structural defects which could broaden the localized and extended states creating a smaller energy band gap [21- 22].

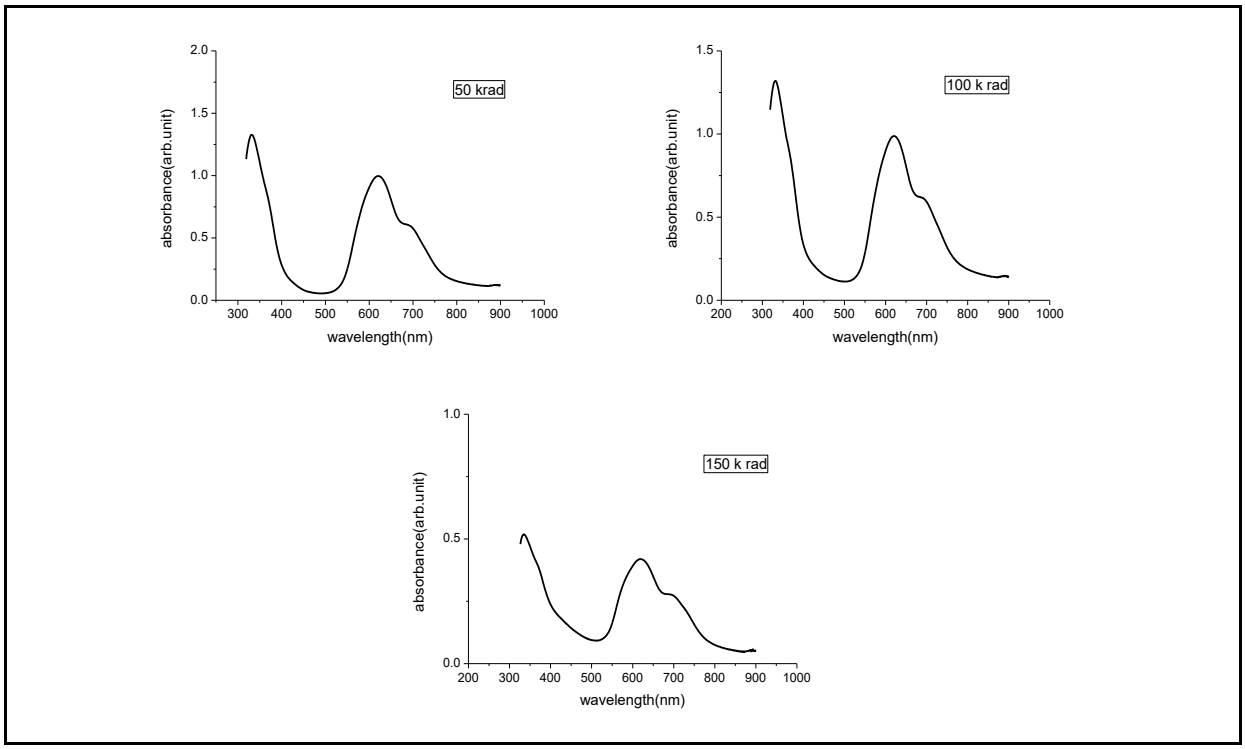

Fig. 3.2 Plot of absorption spectra of H_2PcOC_8 thin film having thickness 250 ± 5 nm irradiated with different dosage of gamma radiation

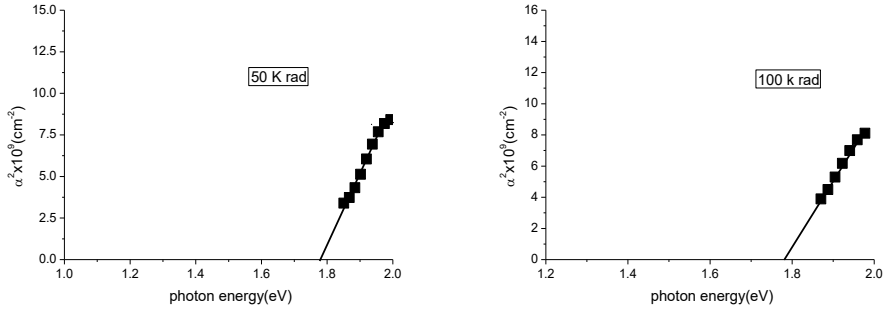

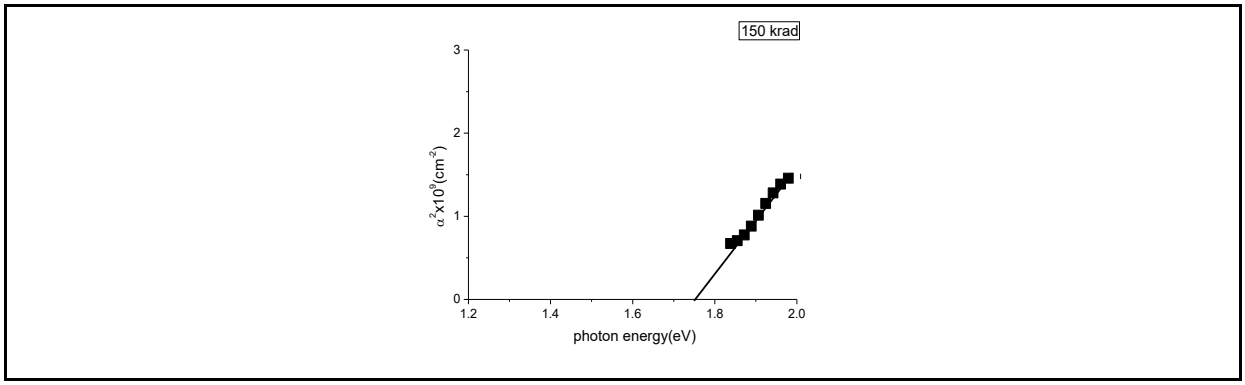

Fig. 3.3 α^2 versus energy graphs for H_2PcOC_8 thin film of thickness 250 ± 5 nm irradiated with different gamma radiation dosages (Q-band)

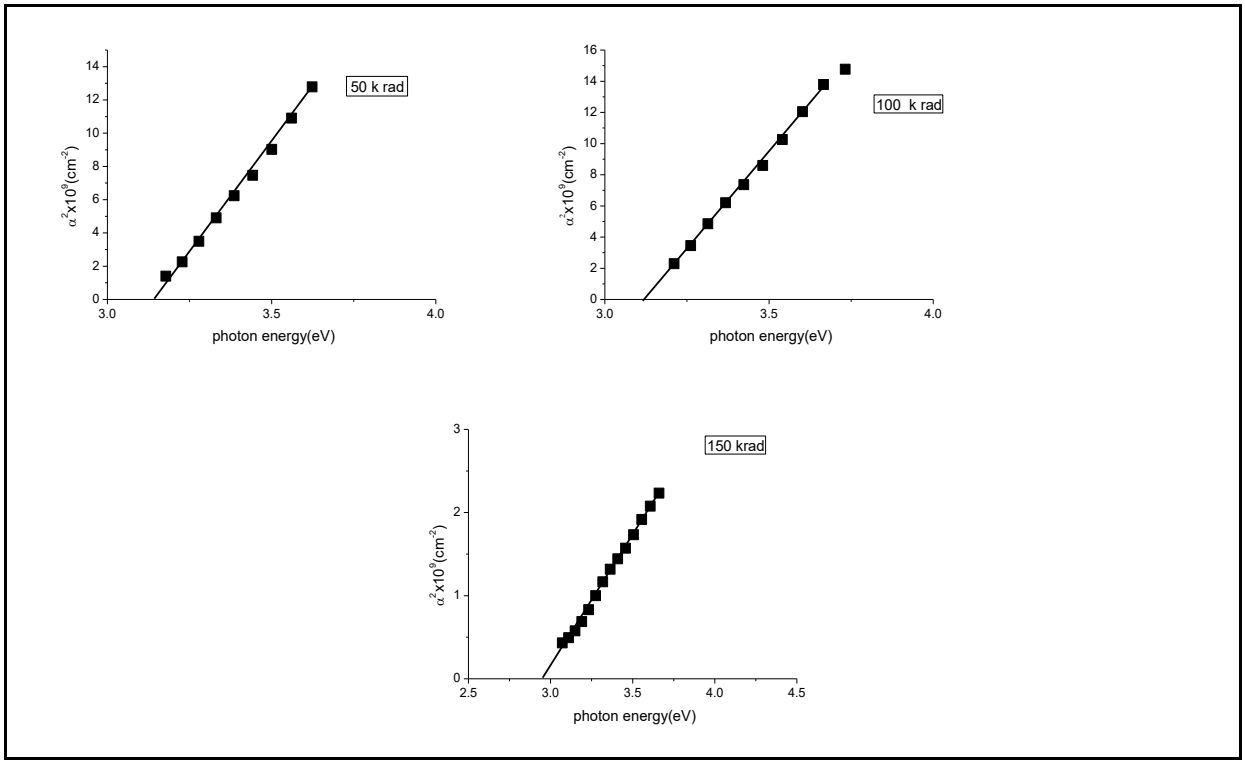

Fig. 3.4 α^2 versus energy graphs for H_2PcOC_8 thin film of thickness 250 ± 5 nm irradiated with different gamma radiation dosages (B- band)

Table 3.1 Variation of Excitonic and Fundamental energy gap of H_2PcOC_8 thin films of thickness 250 ± 5 nm as a function of gamma irradiation dosage

Radiation Dosage (k rad)	Excitonic energy gap Eg_1± 0.01 eV	Fundamental energy gap Eg_2 ± 0.01 eV
50	1.78	3.14
100	1.78	3.12
150	1.75	2.95

3.4.1.2 $ZnPcOC_8$ thin films

The optical absorption spectra of $ZnPcOC_8$ thin films of thickness 250 ± 5 nm irradiated with different γ radiation dosages is shown in Figure 6.5. The corresponding α^2 versus hυ graph for excitonic and fundamental gap is shown in Figure 6.6 and 6.7. The intensity of the absorption peak is almost the same in three dosages. All the samples possess a B- band near 330 nm and a broad Q- band in the range 630- 740 nm. Here the Q- band broad.The broadening of the absorption band is due to the aggregation of molecules [23]. The values of excitonic and fundamental energy gap of the $ZnPcOC_8$ thin films are tabulated in Table 6.2. The value of fundamental band gap increased to 3.18 eV from its as deposited

value of 3.13 eV (Figure 4.7). Also on γ irradiation the band gap energy reduces to 3.05 eV for a radiation dosage of 150 k rad.

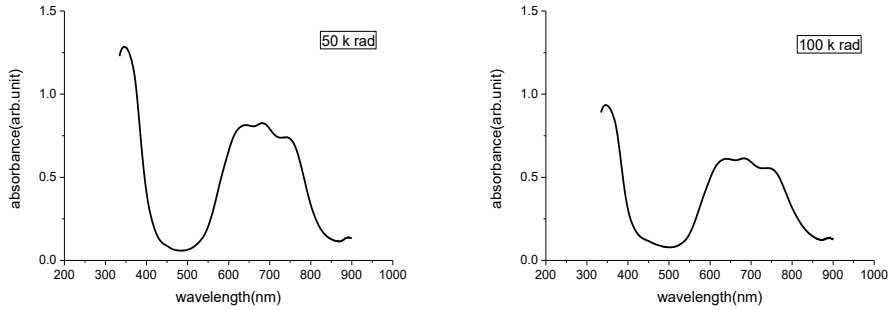

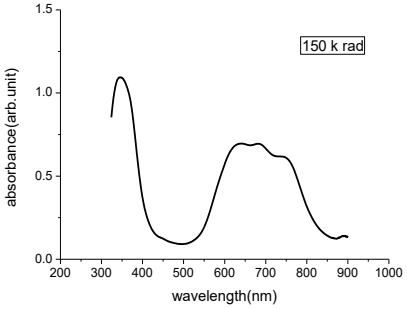

Fig. 3.5 Plot of absorption spectra of $ZnPcOC_8$ thin film having thickness 250 ± 5 nm irradiated with different dosage of gamma radiation

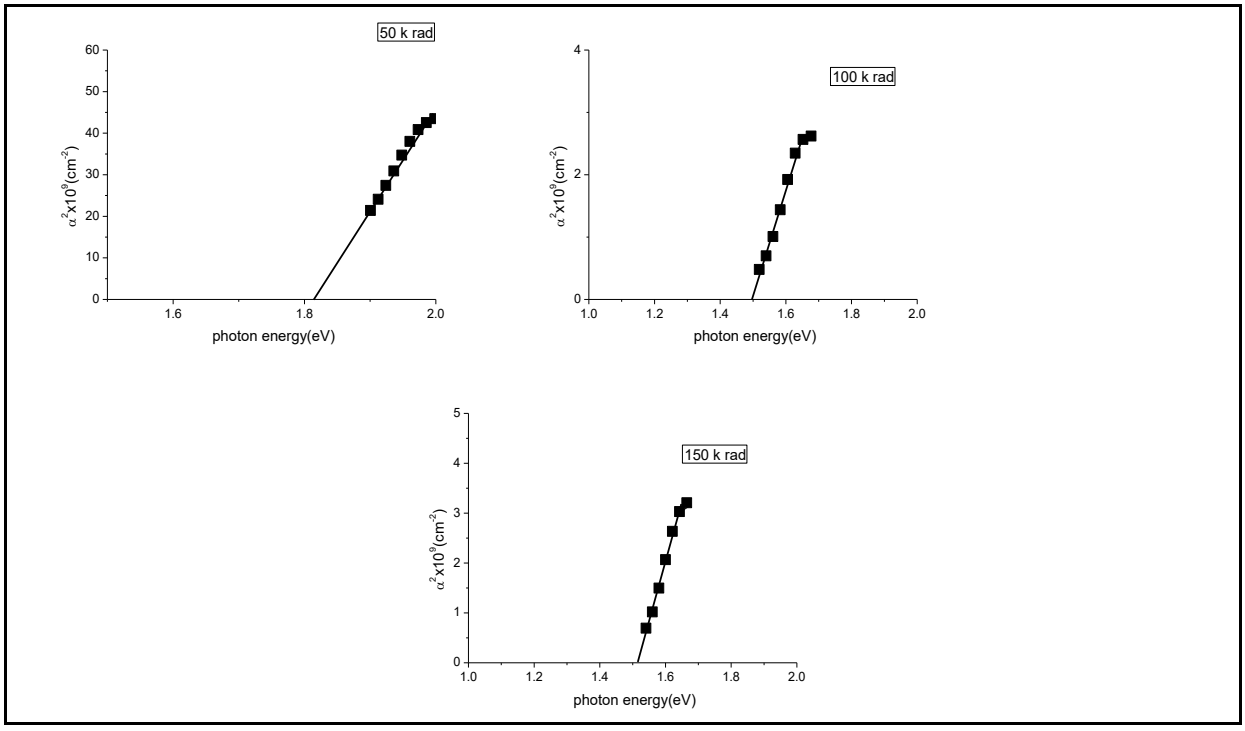

Fig. 3.6 α^2 versus energy graphs for $ZnPcOC_8$ thin film of thickness 250 ± 5 nm irradiated with different gamma radiation dosages (Q-band)

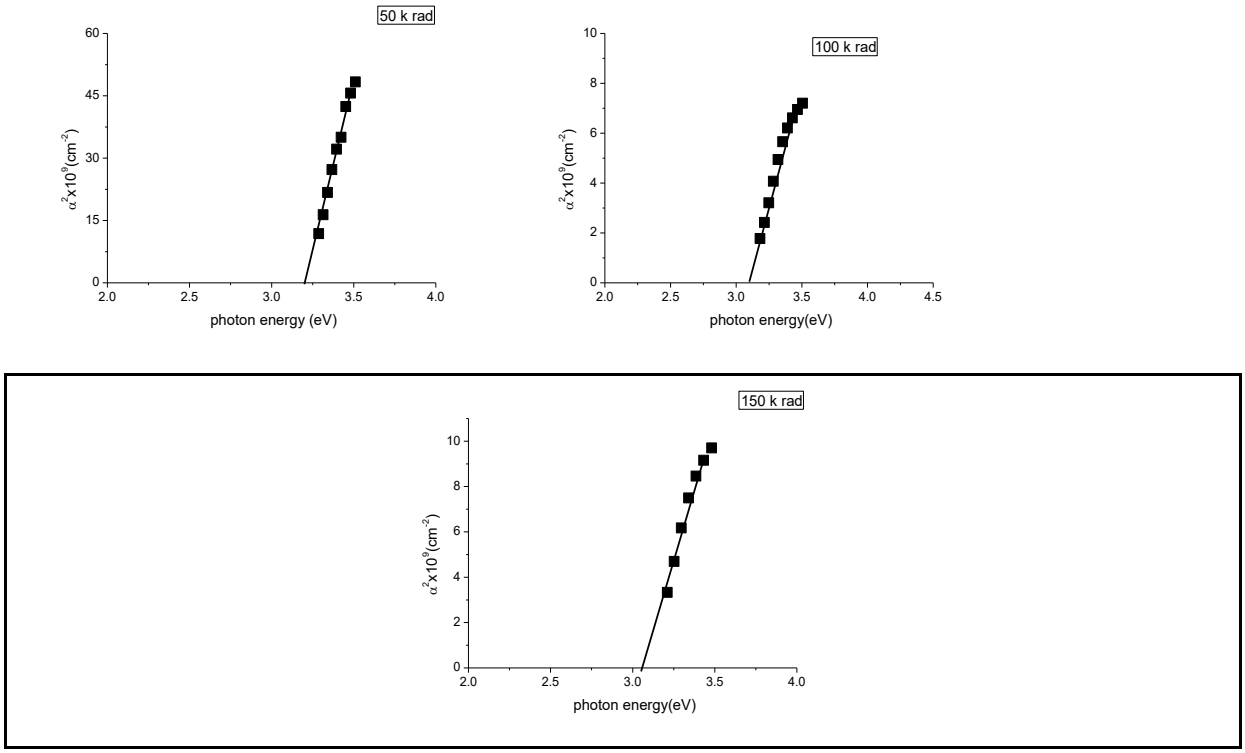

Fig. 3.7 α^2 versus energy graphs for $ZnPcOC_8$ thin film of thickness 250 ± 5 nm irradiated with different gamma radiation dosages (B- band)

Table 3.2 Variation of Excitonic and Fundamental energy gap of $ZnPcOC_8$ thin films of thickness 250 ± 5 nm as a function of gamma irradiation dosage

Radiation Dosage (k rad)	Excitonic energy gap $Eg_1 \pm 0.01$ eV	Fundamental energy gap $Eg_2 \pm 0.01$ eV
50	1.81	3.18
100	1.50	3.08
150	1.51	3.05

3.4.1.3 $CuPcOC_8$ thin films

Figure 6.8 shows the UV- Visible spectral behaviour of absorbance of the $CuPcOC_8$ thin films with thickness 250 ± 5 nm irradiated with γ ray of radiation dosages 50 k rad, 100 k rad and 150 k rad. Intensity of the absorption peak is low for 150 k rad radiation dosage. The figure shows two absorption bands. The absorption at 350 nm is identified as the Soret band and the absorption in the range 610- 697 nm is the Q- band. Figure 6.9 and 6.10 shows the variation of α^2 with photon energy for the excitonic gap and fundamental gap of the $CuPcOC_8$ thin films. The corresponding energy values are enlisted in Table 6.3. There is no appreciable variation in band gap with γ irradiation. This shows the optical band gap of $CuPcOC_8$ thin film is stable upon high–energy radiation. Similar results are obtained for Vanadyl 2- 3 naphthalocyanine and tin phthalocyanine thin films [24- 25].

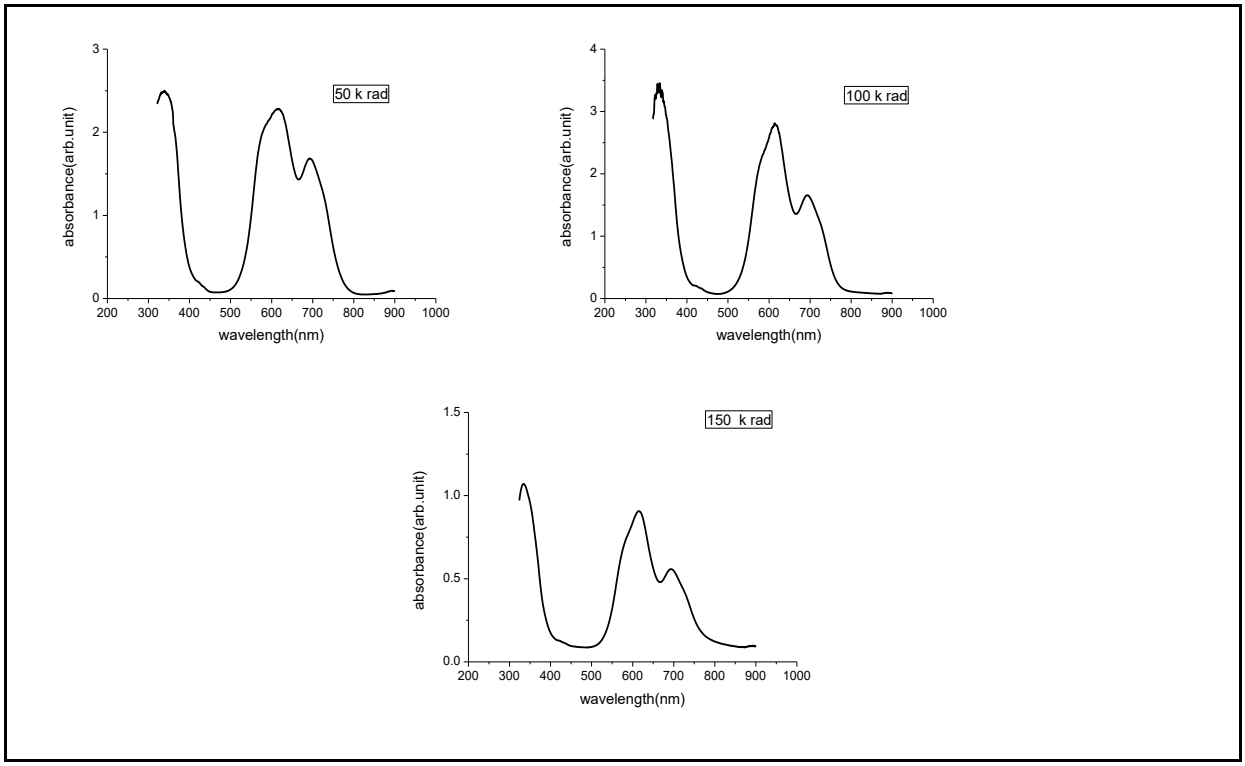

Fig. 3.8 Plot of absorption spectra of $CuPcOC_8$ thin film having thickness 250 ± 5 nm irradiated with different dosage of gamma radiation

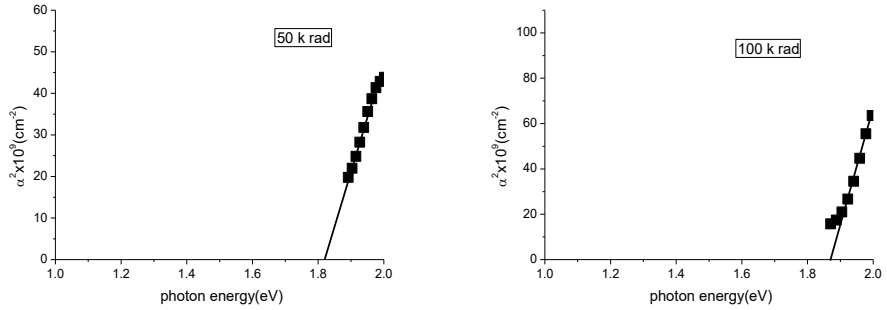

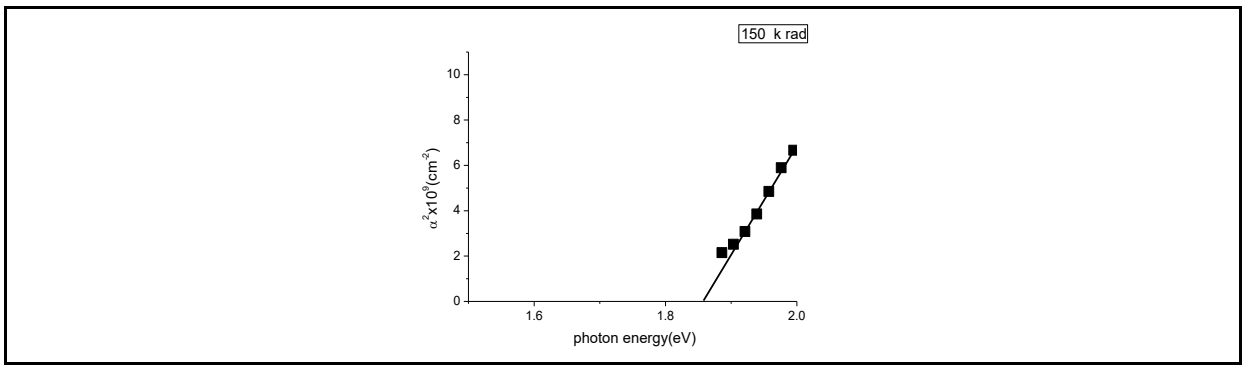

Fig. 3.9 α^2 versus energy graphs for $CuPcOC_8$ thin film of thickness 250 ± 5 nm irradiated with different gamma radiation dosages (Q- band)

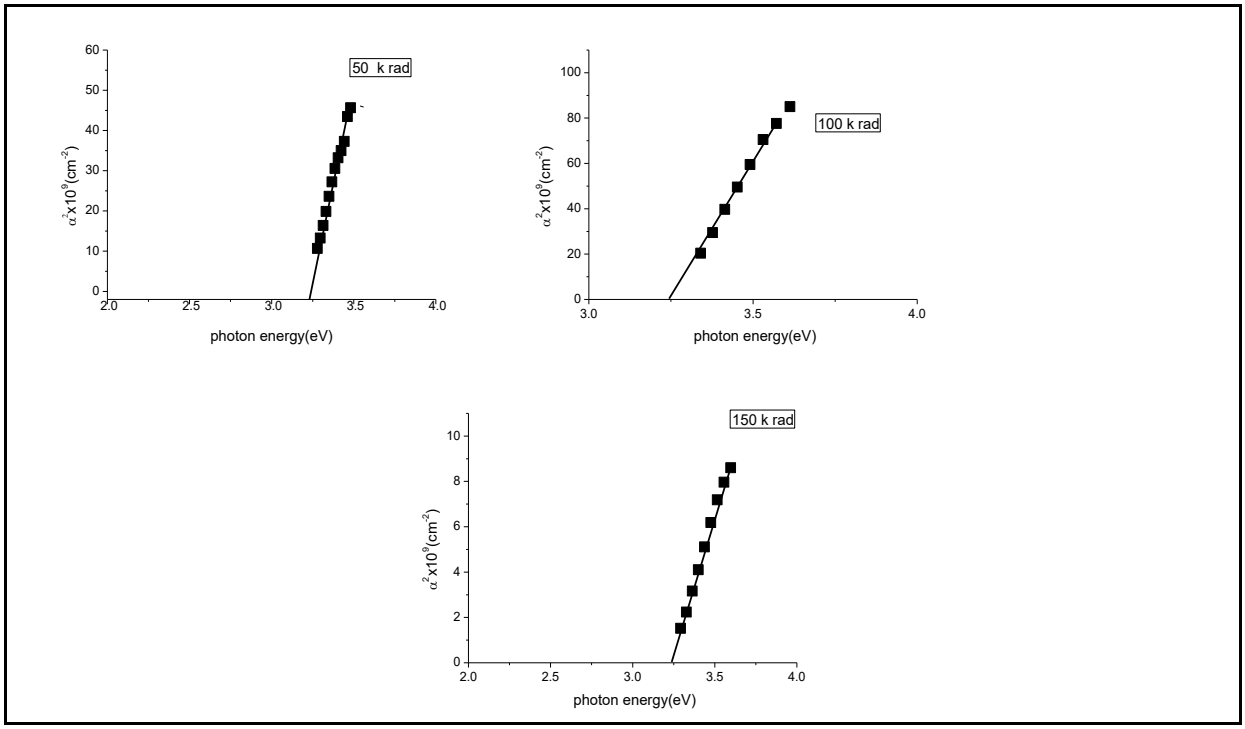

Fig. 3.10 α^2 versus energy graphs for $CuPcOC_8$ thin film of thickness 250 ± 5 nm irradiated with different gamma radiation dosages (B-band)

Table 3.3 Variation of Excitonic and Fundamental energy gap of $CuPcOC_8$ thin films of thickness 250 ± 5 nm as a function of gamma irradiation dosages

Radiation Dosage (k rad)	Excitonic energy gap $Eg_1 \pm 0.01$ eV	Fundamental energy gap $Eg_2 \pm 0.01$ eV
50	1.81	3.24
100	1.87	3.23
150	1.85	3.23

3.4.2 Electrical studies

Electrical properties of organic semiconductor thin films strongly depend on the conditions of deposition and post deposition treatments. For the substituted and non substituted Pc thin films, the electrical conductivity σ fulfils the Arrhenius equation:

$$\sigma = \sigma_0 exp\left({}^{E}/_{K_B T}\right) \qquad 6.4.2.1$$

Where σ is the conductivity at the temperature T (K), E is the thermal activation energy, K_B is the Boltzmann constant and σ_0 is the pre- exponential factor. The Arrhenius plot (ln σ vs 1000/T) yields a straight line, with slope corresponding to the value of thermal activation energy

3.4.2.1 H_2PcOC_8 thin films

In Figure 6.11, ln σ vs 1000/T is plotted for H_2PcOC_8 thin films of thickness 250 ± 5 nm after irradiated with different γ radiation dosages. According to Davis and Mott [26], in this type of material the conductivity exhibits different behaviour in various regions of the Arrhenius plot. There are three linear regions for each graph, which give three activation energies E_1, E_2 and E_3. The activation energy E_1 is related to the intrinsic generation process and E_2 and E_3 to the impurity scattering [18]. The conduction mechanism at low temperature is explained in terms of hopping through a band of localized states and at higher temperatures- in terms of thermal excitation of carriers to the band edges. The change in the slope, and hence the change in the activation energy, reflects a change from intrinsic conduction to the extrinsic one [27]. The activation energies determined for irradiated samples are listed in Table 6.4. The activation energy increases with exposure of gamma radiation. Thus irradiation of the samples with high- energy radiation creates structural defects which act as trapping centres. This is indicated by the increase of activation energy and thus the reduction in the conductivity of H_2PcOC_8 thin films.

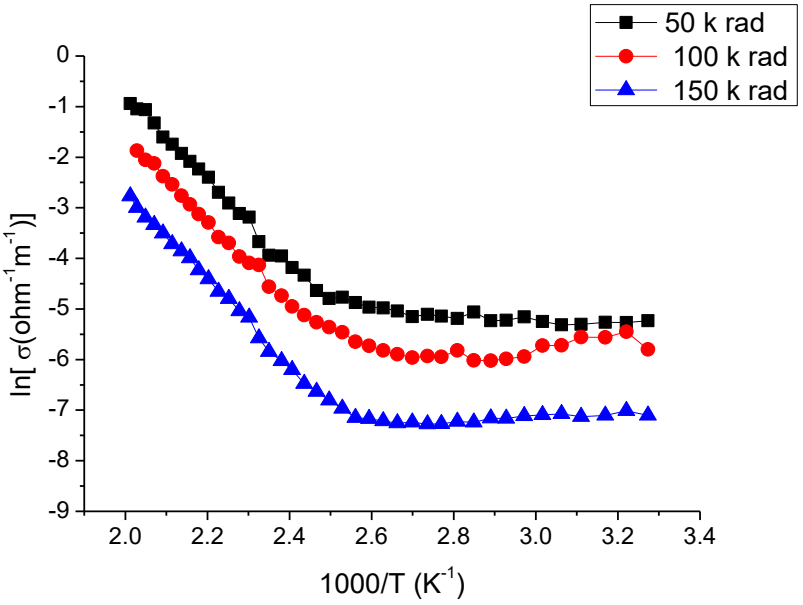

Fig. 3.11 Plot of ln σ vs 1000/T for the H_2PcOC_8 thin films of thickness 250 ± 5 nm irradiated with different gamma radiation dosages

Table 3.4 Variation of activation energy in the intrinsic and extrinsic region as a function of gamma irradiation dosage for the H_2PcOC_8 thin films of thickness 250 ± 5 nm

Radiation dosage (k rad)	Activation energy(eV ± 0.01 eV)		
	E_1	E_2	E_3

50	0.70	0.31	0.02
100	0.72	0.35	0.03
150	0.75	0.37	0.06

3.4.2.2 $ZnPcOC_8$ thin films

Plotting ln σ versus 1000/T yielded a straight line whose slope can be used to determine the thermal activation energy of the film. Figure 6.12 plots the ln σ versus 1000/T graphs for the gamma irradiated $ZnPcOC_8$ thin films of thickness 250 ± 5 nm. Each curve contains three linear regions relating to the three activation energies E_1, E_2 and E_3 and could be interpreted as the difference between dominant energy levels [28]. In substituted phthalocyanines the conductivity is strongly temperature dependent and the charge carrier transport mechanism is generally of free band type in the higher region and of hopping type in the low- temperature region [29]. The activation energies determined for irradiated samples are listed in Table 6.5. The activation energy increases with exposure up to 100 k rad and then decreases. The reduction in activation energy at 150 k rad may be attributed to the instability of the material due to heavy vibrations of the atoms.

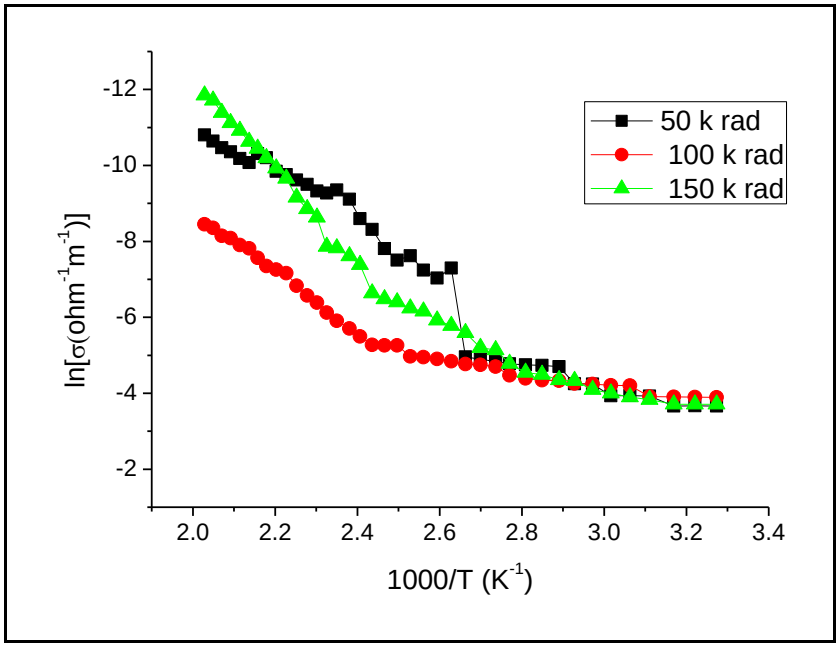

Fig. 3.12 Plot of ln σ vs 1000/T for the $ZnPcOC_8$ thin films of thickness 250 ± 5 nm irradiated with different gamma radiation dosages

Table 3.5 Variation of activation energy in the intrinsic and extrinsic region as a function of gamma irradiation dosage for the $ZnPcOC_8$ thin films of thickness 250 ± 5 nm

Radiation dosage (k rad)	Activation energy(eV ± 0.01 eV)

	E_1	E_2	E_3
50	0.69	0.41	0.06
100	0.77	0.45	0.05
150	0.55	0.39	0.06

3.4.2.3 $CuPcOC_8$ thin films

Figure 6.13 shows the ln σ versus 1000/T plots of $CuPcOC_8$ thin films of thickness 250 ± 5 nm irradiated with different γ radiation dosages. Each curve contains three linear regions relating to three activation energies E_1, E_2 and E_3.The values of which are collected in Table 6.6. From the table it is clear that as the radiation dose increases, the activation energy also increases. The maximum value obtained is 0.68 for 150 k rad. The conductivity for all the $CuPcOC_8$ thin films was found to have much higher values, especially at the high temperature region. This indicates a production of large number of thermally activated charge carriers in vacuum deposited films under investigation. From the table it is clear that the 50 k rad irradiated sample has a higher conductivity values at the high temperature region compared to the one irradiated at 150 k rad. The higher conductivity values for moderate γ irradiation at 50 k rad might be due to the weakening of interaction forces between atoms due to the introduction of lattice defects or due to the ionization effects leading to the presence of internal bias [30- 31].

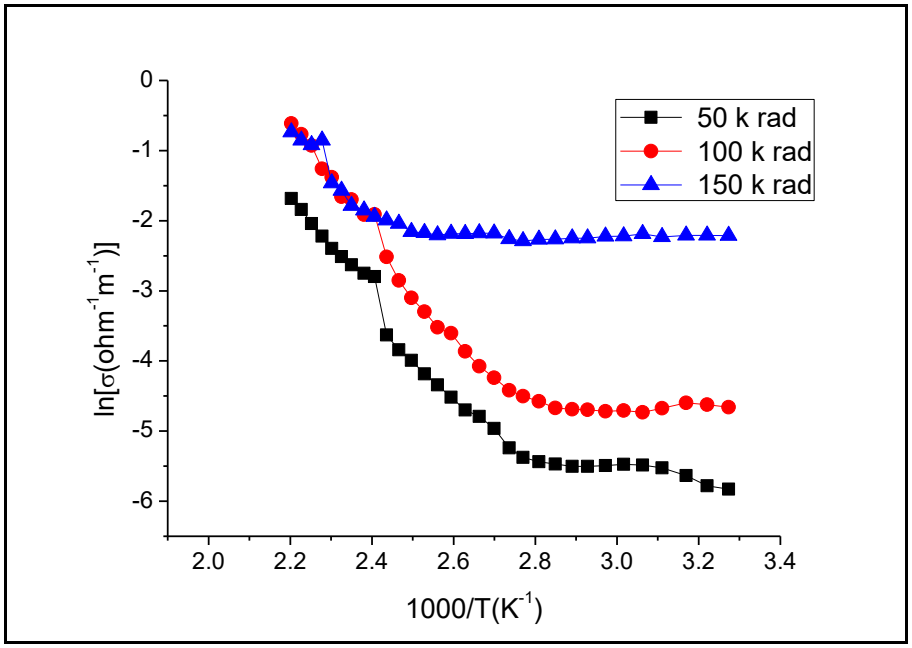

Fig. 3.13 Plot of ln σ vs 1000/T for the $CuPcOC_8$ thin films of thickness 250 ± 5 nm irradiated with different gamma radiation dosages

Table 3.6 Variation of activation energy in the intrinsic and extrinsic region as a function of gamma irradiation dosage for the $CuPcOC_8$ thin films of thickness 250 ± 5 nm

Radiation dosage (k rad)	Activation energy(eV ± 0.01 eV)		
	E_1	E_2	E_3
50	0.44	0.31	0.02
100	0.59	0.35	0.03
150	0.68	0.37	0.06

3.5 Photoluminescence studies

All solids, including semiconductors, have so- called "energy gaps" for the conduction electrons. If a light particle (photon) has energy greater than the band gap energy, then it can be absorbed and thereby raise an electron from the valence band up to the conduction band across the forbidden energy gap (Figure 4.45)

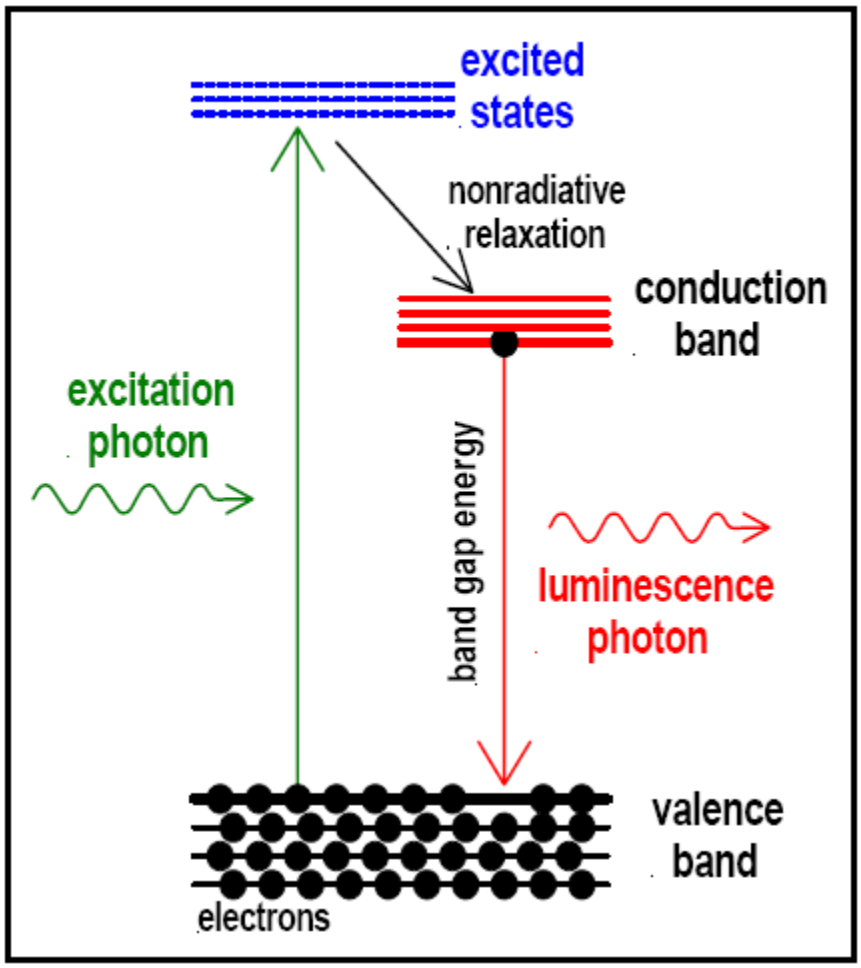

Fig. 3.14 Schematic representation of photoluminescence

In this process of photoexcitation, the electron generally has excess energy which it loses before coming to rest at the lowest energy in the conduction band. At this point the electron eventually falls back down to the valence band. As it falls down, the energy it loses is converted back into a luminescent photon which is emitted from the material. Thus the energy of the emitted photon is a direct measure of the band gap energy. The process of photon excitation followed by photon emission is called photoluminescence. Thus photoluminescence (PL) is the spontaneous emission of light from a material under optical excitation the excitation energy and intensity are chosen to probe different regions and excitation concentrations in the sample. PL investigations can be used to characterize a variety of material parameters. Features of the emission spectrum can be used to identify surface, interface, and impurity levels and to gauge alloy disorder and interface roughness. The intensity of the PL signal provides information on the quality of surfaces and interfaces. PL depends on the nature of the optical excitation. The excitation energy selects the initial photo excited state and governs the penetration depth of the incident light. The PL signal often depends on the density of the photo excited electrons and the intensity of the incident beam can be adjusted to control this parameter.

Thin films of H_2PcOC_8, $ZnPcOC_8$ and CuPcOC8 are annealed in air for one hour under identical conditions but at different temperatures 323 K, 473 K, and 523 K. The emission spectra at room temperature are recorded by a Spectrophotometer (RF- 5301 PC, Shimadzu, Japan). The samples are kept at about 45° angle with the incident photoexcitation light beam for preventing the reflected rays to reach the photodetector of the spectrophotometer during the recording of the emission spectra. The PL spectra of the H_2PcOC_8 (photoexcitation at 325 nm), $ZnPcOC_8$ (photoexcitation at 341 nm) and $CuPcOC_8$ (photoexcitation at 331 nm) thin films of thickness 250 ± 5 nm annealed in air at different temperatures are shown in Figures 4.46, 4.47 and 4.48 respectively.

For the H_2PcOC_8 sample, it is clear that at low temperatures there is no photoemission. For the film annealed at 523 K, small broad peak is centered on 448 nm- 497 nm is observed.

From the PL spectrum of $ZnPcOC_8$ and $CuPcOC_8$ thin films (Figure 4.47 and 4.48), it is observed that the as deposited film doesn't show any emission peaks. But as the annealing temperature increases small peaks with broad band is observed. In the case of $ZnPcOC_8$ the peaks are centered at 440 nm to 512 nm whereas in the case of $CuPcOC_8$, it is around 447 nm – 500 nm. The profiles of the PL spectra of $ZnPcOC_8$ and $CuPcOC_8$ samples are almost

similar in nature. With increase in annealing temperature, much better profiles of PL spectra are observed. In general, the profile of the PL spectrum depends on the annealing temperature.

Development of the structures is a clear indication of a decrease in size quantum–confined semiconductor particles [43]. The observation of structure is characteristic for narrow size distribution. It is reported [43] that particles with very narrow size distribution can exhibit broad absorption and emission bands once they are in the strong confinement regime. The more complex shape of emission spectrum suggests that the clusters have more defects [44]. The similarities in the shape of the emission peaks may indicate some correlation in the surface properties or incidence of defects [45].

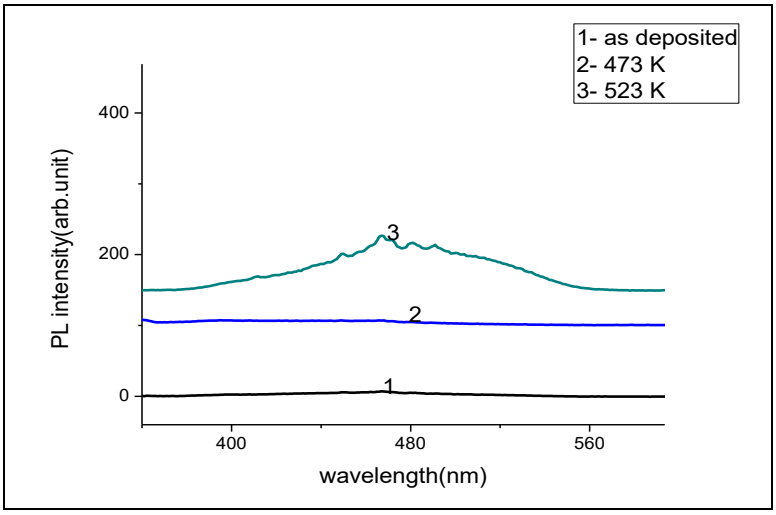

Fig. 3.15 PL spectra of the H_2PcOC_8 thin film of thickness 250 ± 5 nm annealed in air at different temperatures for photoexcitation wavelength 325 nm

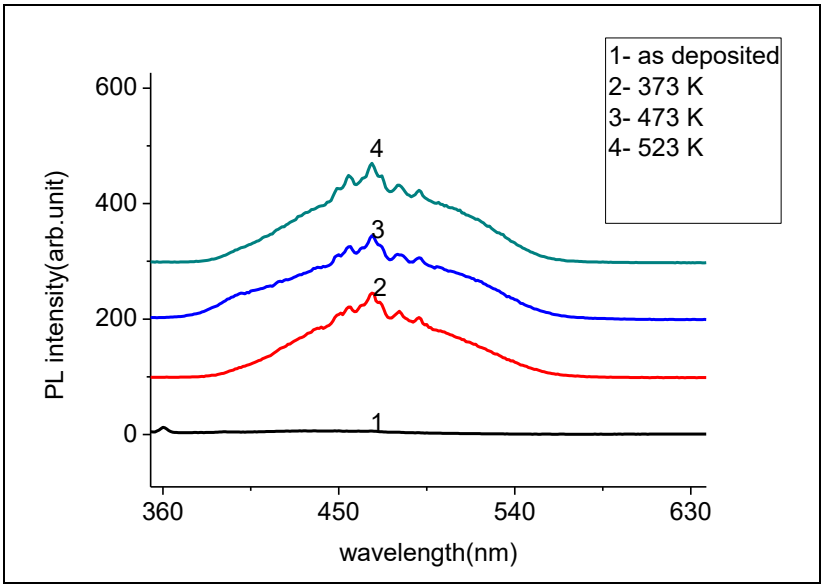

Fig. 3.16 PL spectra of the $ZnPcOC_8$ thin film of thickness 250 ± 5 nm annealed in air at different temperatures for photoexcitation wavelength 341 nm

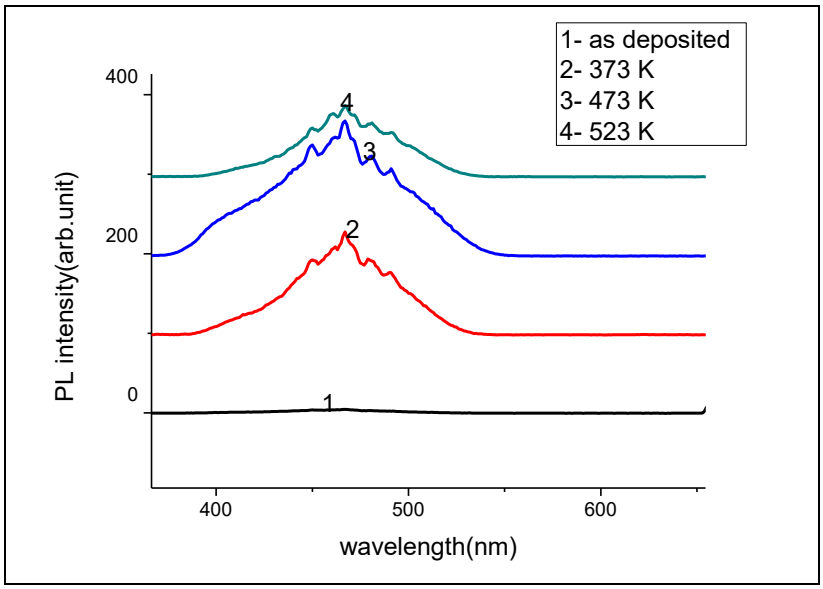

Fig. 3.17 PL spectra of the $CuPcOC_8$ thin film of thickness 250 ± 5 nm annealed in air at different temperatures for photoexcitation wavelength 331 nm

3.6 Conclusion

Thin films of H_2PcOC_8, $ZnPcOC_8$ and $CuPcOC_8$ are prepared by vacuum deposition method. The prepared films are γ irradiated with a dosage of 50 k rad, 100 k rad and 150 k rad to study the variation of its optical and electrical properties. The results of the optical properties of H_2PcOC_8, $ZnPcOC_8$ and $CuPcOC_8$ after γ irradiation have been studied in the spectral range 200- 900 nm. The recorded absorption spectra in the UV- Vis region have two absorption bands, the Soret (B- band) and the splitting Q- band. These absorption spectra are generally interpreted in terms of π- π^* transition. As observed, a slight difference in the absorption coefficient spectra for the as deposited and irradiated films may be due to the little change in the optical density. It is found that the optical band gap of H_2PcOC_8 thin films decreases by γ irradiation, which can be attributed to some variations in disorder and lattice defect system present in the materials. The optical band gap of $ZnPcOC_8$ increases with gamma irradiation, whereas for $CuPcOC_8$ thin films, the optical band gap is stable. It is clearly observed that irradiation attenuates the absorption peaks in all the three materials. Such trend indicates that γ irradiation can induce defects into the bulk or thin film. The thermal activation energy, which determines the minimum energy required to produce a charge carrier in the solid matrix, of the H_2PcOC_8, $ZnPcOC_8$ and $CuPcOC_8$ thin films irradiated with gamma rays is calculated from the electrical conductivity data to understand

the conduction mechanism in these materials. All the three materials showed much higher conductivity in the low temperature region. The Arrhenius plots of these materials shows three linear regions corresponding to the three activation energies E_1, E_2 and E_3. For the H_2PcOC_8 thin films, as radiation dose increases, the activation energy also increases. This is due to the formation of structural defects by the high energy radiation. In the case of $ZnPcOC_8$, the activation energy increases with exposure up to 100 k rad and then decreases. This reduction may be due to the instability of the material due to heavy vibration of the atoms. The charge carriers in Pc are thermally generated holes and the presence of traps plays a dominant role in the conduction of these materials. Presence of trap level is attributed to defects generated by ambient nitrogen, hydrogen and oxygen affecting electrical conductivity, mobility and trap density. Structural defects may also affect the conductivity. This in turn affects the position of Fermi level. During the irradiation of $ZnPcOC_8$ samples with high energy radiation creates structural defects which act as trapping centres. This is indicated by the increase of activation energy and thus the reduction in the conductivity of the $ZnPcOC_8$ thin films. In the case of $CuPcOC_8$ thin films, as the radiation dose increases the activation energy increases and hence the conductivity decreases. The 50 k rad irradiated sample has a higher conductivity values at the high temperature region compared to the one irradiated at 150 k rad. The responsible factor for this change is solely due to the change in concentration of charge carriers induced by the irradiation energy. The higher conductivity values for a moderate γ irradiation at 50 k rad might be due to the weakening of interaction forces between atoms due to the introduction of lattice defects or due to the ionization effects leading to the presence of internal bias. However at 150 k rad the induced defects might have recombined showing lower conductivity values. Thus in general irradiation with γ rays can change both the values of electrical conductivity and its temperature dependence due to the creation of point defects by the direct interaction of Compton electrons with lattice atoms and by multiple collisions. Also there are chances of formation of short lived free radicals upon irradiation.

References

1. Holmes- Siedle, A.G., L. Adams, Handbook of Radiation Effects, New York, Oxford University Press, 1993.
2. Chopra K.L., Thin Film Phenomena, Malabar F.L., Robert E. Krieger, 1979.
3. Heavens O.S., Optical Properties of Thin Solid Films, New York, Dover, 1991.
4. Mott N.F., E.A. Davis, Electronic Process in Non- Crystalline Materials, Oxford, U.K., Clarendon, 1979.
5. Mott N.F., Conduction in Non- Crystalline System, Phil. Mag., Vol. **19,** pp. 8–35,1969.
6. Mott N.F., Conduction in Non- Crystalline Materials, Oxford, U.K., Clarendon, 1997.
7. Jonscher A.K., Thin Solid Films, **1**, 213, 1967.
8. Atanassova E., Pasksleva A., Konakova R., Spassov D., Mitin V.F., J. Microelectron, **32**, 553, 2001.
9. Clough R.L., Nucl. Instrum. Meth., **185**, 8, 2001.
10. Ibrahim A.M., Soliman L.I., Rad. Phys. Chem., **53**, 469, 1998.
11. Colby E., Lum. G., Plettner. T., Spencer J., IEEE Trans. Nucl. Sci., **49**, 2857, 2002.
12. Arshak A., Zleetni S., Korostynska O., IEEE Trans. Nucl. Sci., **51**, 2250, 2004.
13. Arshak A., Korostynska O., Mater. Sci. Eng., **133**, 1, 2006.
14. Arshak A., Korostynska O., Molly J., Harris J., IEEE Sens. J., **6**, 656, 2006.
15. Kumar G.A., Maity T.K., Kumar A., Sharma S.L., Int. Conf. on advances in Materials and Processing, ICAMMP (Kharagpur IIT), 2006, p. 913.
16. Maity T.K., Sharma S.L., Bull. Mater. Sci., **31**, 841, 2008.
17. Sharma S.L., Maity T.K., Kumar G.A., IEEE- NSS Conf. Record, **281**, 1066, 2008.
18. Collins R.A., Krier A., Abass A.K., Thin Solid Films, **229**, 113, 1993.
19. El- Nahass M.M., Abd- El- Rahman K.F., Al- Ghamd A.A., Asiri A.M. Physica. B, **344**, 398, 2004.
20. Bardeen J., Slatt F.L., Hall L.T., Photoconductivity Conf., Wiley, New York, 1965.
21. Arshak A., Zleetini S., Arshak K., Sensors, **2**, 174, 2002.

22. Yaghmour S. J., J. Alloys Compd., **486**, 284, 2009.

23. Bajema L., Gouterman M., Rose C.B., J. Mol. Spectrosc., **33**, 292, 1971.

24. Nisha S.P., Menon C.S., J. Mater. Sci., **46**, 4479, 2011.

25. Regimol C.C., Menon C.S., Material Science Poland, **25**, 649, 2007.

26. Mott N.F., Davis E.A., Electronic Processes in Non- Crystalline Materials, Oxford University Press, Oxford, 1979.

27. Hassan A.K., Gould R.D., J. Phys. Condens. Matter., **1**, 6679, 1998.

28. Belghachi A., Collins R.A., J. Phys. D., **21**, 1647, 1988.

29. Vidadi Y.A., Rozenshetein L.D., Chistyakov E.A., Sov. Phys. Sol. Stat., **11**, 219, 1969.

30. Ahammed M.A., Summan A.M., Mousa M.A., J. Mater. Sci- Mater. Electron, **2**, 1, 1992.

31. Gaffar M.A., Hussien A.G., J. Phys. Chem. Solids, **62**, 2011, 2001.

CHAPTER 4

SUMMARY AND CONCLUSION

This project presents with the electrical, optical and structural properties of the thin films of 2, 3, 9, 10, 16, 17, 23, 24 Octakis (octyloxy) Phthalocyanine (H_2PcOC_8), 2, 3, 9, 10, 16, 17, 23, 24 Octakis (octyloxy) Zinc Phthalocyanine ($ZnPcOC_8$), 2, 3, 9, 10, 16, 17, 23, 24 Octakis (octyloxy) Copper Phthalocyanine ($CuPcOC_8$) and the effect of gamma irradiation. Varying parameters like thickness, annealing temperature and irradiation with suitable dosages of gamma rays are imposed on all the three materials to study their improvement for achieving better performance. The analysis of the photoluminescence (PL) spectra is also

done. The implications of the investigations and conclusions derived from are summarised. The scope of future work is also indicated.

The state- of- art knowledge on different features of the substituted phthalocyanines has been reviewed in the opening chapter in such details as is required for the proper understanding of the work presented in subsequent chapters.

The physical properties of substituted and non substituted Pcs thin films are strongly influenced by their particle growth and the post deposition thermal treatment and irradiation with higher energetic radiations like gamma radiation which is expected to affect their internal structure and consequently on their physical properties. The results of the optical properties of the H_2PcOC_8, $ZnPcOC_8$ and $CuPcOC_8$ thin films irradiated with γ rays are presented in the spectral range of 200- 900 nm. The recorded absorption spectra in the UV-Vis regions have two absorption bands, the Soret band and the splitting Q- band. These absorption spectra are generally interpreted in terms of π- π^* excitation. It is found that for H_2PcOC_8 and $ZnPcOC_8$ thin films, the optical band gap decreases with γ irradiation. This is due to the lattice defects present in the material, which is known to increase the width of the localized states, and reduce the optical band gap. But for $CuPcOC_8$ thin films, on γ irradiation, the band gap energy has reduced to 3.24 eV but remains almost stable for all irradiation dosages. Since the γ irradiation brings about changes within the film matrix by inducing structural defects which could broaden the localized and extended states. Effects of gamma radiation on the electrical properties of H_2PcOC_8, $ZnPcOC_8$ and $CuPcOC_8$ thin films reveal that, all the films show much higher conductivity in the high temperature region. The Arrhenius plots of all the three materials show three linear regions corresponding to which the three activation energies are observed. It is found that the activation energy of the three materials vary with γ irradiation. For H_2PcOC_8 and $CuPcOC_8$ thin films the activation energy increases with exposure to gamma radiation. Thus for H_2PcOC_8 and $CuPcOC_8$ thin films, the irradiation creates structural defects which in turn reduces the conductivity of the films. But for $ZnPcOC_8$ thin films the activation energy increases up to 100 k rad and then decreases. This reduction is due to the instability of the material due to large vibrations of the atoms. Thus the study of the irradiated films increases their applicability in different fields and enables information about the induced irradiation defects and their interaction with matter.

The analysis of PL spectra shows that the small and wide PL peak arises due to the defects present in the three materials. The change in the profile shows that the effect of annealing is

significantly related to the nature of the surface morphology of the H_2PcOC_8, $ZnPcOC_8$ and $CuPcOC_8$ thin films.